Distinct proteostasis states drive pharmacologic chaperone susceptibility for cystic fibrosis transmembrane conductance regulator misfolding mutants

Eli Fritz McDonald[a,†], Carleen Mae P. Sabusap[a,†], Minsoo Kim[a,b], and Lars Plate[a,c,*]
[a]Department of Chemistry, [b]Chemical and Physical Biology Program, [c]Department of Biological Sciences, Vanderbilt University, Nashville, TN, USA

ABSTRACT **Pharmacological chaperones represent a class of therapeutic compounds for treating protein misfolding diseases. One of the most prominent examples is the FDA-approved pharmacological chaperone lumacaftor (VX-809), which has transformed cystic fibrosis (CF) therapy. CF is a fatal disease caused by mutations in the CF transmembrane conductance regulator (CFTR). VX-809 corrects folding of F508del CFTR, the most common patient mutation, yet F508del exhibits only mild VX-809 response. In contrast, rarer mutations P67L and L206W are *hyperresponsive* to VX-809, while G85E is *nonresponsive*. Despite the clinical success of VX-809, the mechanistic origin for the distinct susceptibility of mutants remains unclear. Here we use interactomics to characterize the impact of VX-809 on proteostasis interactions of P67L and L206W and compare these with F508del and G85E. We determine that *hyperresponsive* mutations P67L and L206W exhibit decreased interactions with proteasomal and autophagy degradation machinery compared with F508del and G85E. We then show inhibiting the proteasome attenuates P67L and L206W VX-809 response. Our data suggest a previously unidentified but required role for protein degradation in VX-809 correction. Furthermore, we present an approach for identifying proteostasis characteristics of mutant-specific therapeutic response to pharmacological chaperones.**

Monitoring Editor
Elizabeth Miller
MRC Laboratory of Molecular Biology

Received: Nov 17, 2021
Revised: Mar 24, 2022
Accepted: Mar 28, 2022

INTRODUCTION

The proteostasis network (PN) evaluates the folding fidelity of proteins, allowing trafficking of properly folded proteins to their cellular destination while coordinating degradation of misfolded proteins. Misfolded proteins can be rescued from PN degradation by pharmacological chaperones, an emerging class of small molecule therapeutics that stabilize protein targets. For instance, the pharmacological chaperone Lumacaftor (VX-809) is part of an FDA-approved treatment for cystic fibrosis (CF), one of the most common lethal

This article was published online ahead of print in MBoC in Press (http://www.molbiolcell.org/cgi/doi/10.1091/mbc.E21-11-0578) on April 7, 2022.

†These authors contributed equally to this work.

Conflict of interest: The authors declare that they have no conflict of interest related to this work.

Author contributions: L.P. and C.S. conceived the study and planned the experiments; E.M. and C.S. performed the experiments; E.M., L.P., and C.S. analyzed the data, prepared the figures, and wrote the manuscript; M.K. assisted with experiments and data analysis; L.P., C.S., and M.K. critically reviewed the manuscript; L.P. and E.M. edited the manuscript.

Data availability: The mass spectrometry proteomics data have been deposited to the ProteomeXchange Consortium via the PRIDE partner repository with the dataset identifier PXD032836. All other necessary data are contained within the manuscript.

*Address correspondence to: Lars Plate (lars.plate@vanderbilt.edu).

Abbreviations used: AP-MS, affinity purification-mass spectrometry; CALM1, calmodulin; CANX, calnexin; Co-IP, co-immunoprecipitation; CF, cystic fibrosis; CFTR, cystic fibrosis transmembrane conductance regulator; DERL1, Derlin1; DMSO, dimethylsulfoxide; ER, endoplasmic reticulum; ERAD, ER-associated degradation; GO, gene ontology; LC-MS/MS, liquid chromatography-tandem mass spectrometry; NBD, nucleotide binding domain; PBS, phosphate-buffered saline; PN, proteostasis network; TBS, Tris-buffered saline; TMT, tandem mass tags; TMD, transmembrane domain.

Mendelian diseases in the United States. CF arises from mutations in the CF transmembrane conductance regulator (CFTR) (Okiyoneda *et al.*, 2013; Van Goor *et al.*, 2011; Farinha *et al.*, 2013). CFTR regulates epithelial ion homeostasis necessary for many organ–liquid interfaces and CF patients suffer from altered mucus secretion leading to chronic lung infection, pancreatic and hepatic insufficiency, and premature death (Rowe *et al.*, 2005). Current CF treatment involves stabilizing mutant CFTR with VX-809 (Okiyoneda *et al.*, 2013) to restore protein levels by modulating folding and trafficking. However, VX-809 availability is limited to patients with a small number of mutations that are predicted to have corrector response based on in vitro evaluations typically prioritized based on patient population size (Heijerman *et al.*, 2019; Manfredi *et al.*, 2019; Middleton *et al.*, 2019; Vertex Pharmaceuticals Incorporated, 2020a,b,c).

Among patients with mutations approved for VX-809 treatment, different CFTR mutations exhibit highly variable clinical efficacy (Manfredi *et al.*, 2019). For example, initial CFTR modulators were developed for the most common mutation F508del (Van Goor *et al.*, 2006). F508del represents the prototypical class-II disease-causing mutation leading to altered proteostasis (Wang *et al.*, 2006), trafficking (Farinha and Canato, 2017), and decreased cell surface expression (Hegedus *et al.*, 2006). However, F508del exhibits mild VX-809 rescue relative to other class-II mutations both in vitro (Ren *et al.*, 2013) and among clinical studies (Wainwright *et al.*, 2015). By contrast, the rare mutation P67L, which occurs in less than 300 patients (CFTR2), demonstrates robust VX-809 correction with P67L reaching levels of mature CFTR at the cell surface comparable to wild type (WT) in some cell model systems (Sabusap *et al.*, 2016). Likewise, the mutation L206W responds well to VX-809 in vitro (Veit *et al.*, 2018). Still other mutations, such as G85E, appear to be completely resistant to VX-809 correction in vitro (Lopes-Pacheco *et al.*, 2017). All four mutants also present unique pathobiology in patients with responsive mutants P67L and L206W exhibiting higher residual function than F508del and G85E (Figure 1A). Despite the identical classification of F508del, P67L, L206W, and G85E variants as class-II (abnormal protein folding/trafficking) (Veit *et al.*, 2016), this classification scheme provides little basis for predicting CFTR therapeutic response, otherwise known as *theratype* (Molinski *et al.*, 2017; Clancy *et al.*, 2019). F508del and G85E show similar theratypes with limited to no change in protein levels in response to VX-809 (*moderate* and *nonresponders*) whereas P67L and L206W exhibit dramatic increases in protein levels in response to VX-809 (*hyperresponders*). We sought to understand the underlying proteostasis interactions contributing to CFTR mutant theratype toward the goal of predicting pharmacological chaperone clinical efficacy given a patient mutation.

Previous studies attributed variable VX-809 response to the fundamental folding and/or structural defects conferred by any given mutation (Molinski *et al.*, 2018). Two studies recently converged on a putative VX-809 binding site in the CFTR transmembrane domain 1 (TMD1) (Baatallah *et al.*, 2021; Fiedorczuk and Chen, 2022). However, precisely how changes in structural defects translate to changes in protein expression levels and trafficking efficiency remains unclear. Folding and trafficking of CFTR variants are mediated by changes to quality control processes governed by chaperones, folding, trafficking, and degradation factors comprising the PN. On the one hand, distinct mutations may cause distinct domain level conformational changes leading to changes in chaperone and degradation factor binding affinity (Kim and Skach, 2012; Baaklini *et al.*, 2020). On the other hand, different mutations may experience distinct rate-limiting steps in protein quality control. CFTR protein quality control is dictated by the CFTR-PN protein interactions that regulate the balance between trafficking and degradation (Wang *et al.*, 2006; Pankow *et al.*, 2015). Thus each mutation may get trapped in a specific subcellular locale where the confluence of PN interactors leads to degradation (Horváth *et al.*, 2008; Craig, 2018; Lim *et al.*, 2018). Consequently, it is imperative to understand how VX-809 shapes mutation-specific PN interactions (Coppinger *et al.*, 2012; Hegde *et al.*, 2015). A better mechanistic understanding of this interplay could allow CFTR variant theratyping for future corrector compounds and reveal other potential protein targets for CF treatment.

Past CFTR PN characterization focused on F508del under temperature correction or VX-809 treatment conditions (Pankow *et al.*, 2015; Anglès *et al.*, 2018). Temperature correction to 30°C modulates distinct F508del interactions with Hsp70 and Hsp90 chaperones as well as several degradation factors to enable enhanced trafficking (Baaklini *et al.*, 2020). VX-809 treatment also modulates PN interactions and shifts the F508del interactome toward WT (Hutt *et al.*, 2018). These studies identified chaperones as viable targets for altering CFTR trafficking, demonstrated the broad impact of VX-809 altered proteostasis, but offered little mechanistic insight into the function of VX-809. Few studies have investigated other CFTR mutations, particularly within the context of mutation-specific theratype.

Here we used affinity purification-mass spectrometry (AP-MS) to sensitively detect and quantify CFTR interacting proteins and identify cellular machinery responsible for managing CFTR trafficking or degradation after VX-809 treatment. We quantitatively compared multiple mutants with DMSO and VX-809 treatment by multiplexing AP-MS with isobaric tandem mass tags (TMT) (McAlister *et al.*, 2012). This approach allowed us to sensitively determine interactome changes and PN remodeling under VX-809 treatment for *hyperresponders* P67L and L206W CFTR. We found that *hyperresponsive* mutants shared similar proteostasis interactions to F508del with DMSO—consistent with their common class-II variant classification. However, both *hyperresponsive* mutants showed decreased interactions with proteasomal proteins and autophagy proteins under VX-809 treatment compared with F508del. We then showed that inhibition of the proteasome substantially attenuates the VX-809 response of *hyperresponsive* mutations P67L and L206W as well as partially attenuates the VX-809 response of F508del. These data suggest a previously unidentified role for protein degradation in the VX-809 mechanism. Our multiplexed approach allows for parallel theratyping of additional CFTR variants with other CFTR correctors including recently FDA-approved VX-445 (Heijerman *et al.*, 2019). Furthermore, our methods can be applied to theratyping other protein misfolding diseases to emerging pharmacological chaperone therapies.

RESULTS

Coimmunoprecipitation of VX-809 CFTR variants with differential VX-809 response

We sought to determine how the misfolding CFTR mutants differ in proteostasis interactomes from those of WT. Specifically, we focused on comparing VX-809 *hyperresponders* (P67L, L206W) to *moderate* and *nonresponders* (F508del, G85E) (Figure 1A) to elucidate the mechanisms underlying the divergent VX-809 response. We used coimmunoprecipitation (Co-IP) coupled to LC-MS/MS analysis to isolate CFTR and identify its interacting proteins (Figure 1, B and C) (Pankow *et al.*, 2016). To enable direct, relative comparison of interactor abundance across multiple CFTR variants and in response to corrector treatment, we employed TMT multiplexing (McAlister *et al.*, 2012). Immunoblots confirmed the successful isolation of all

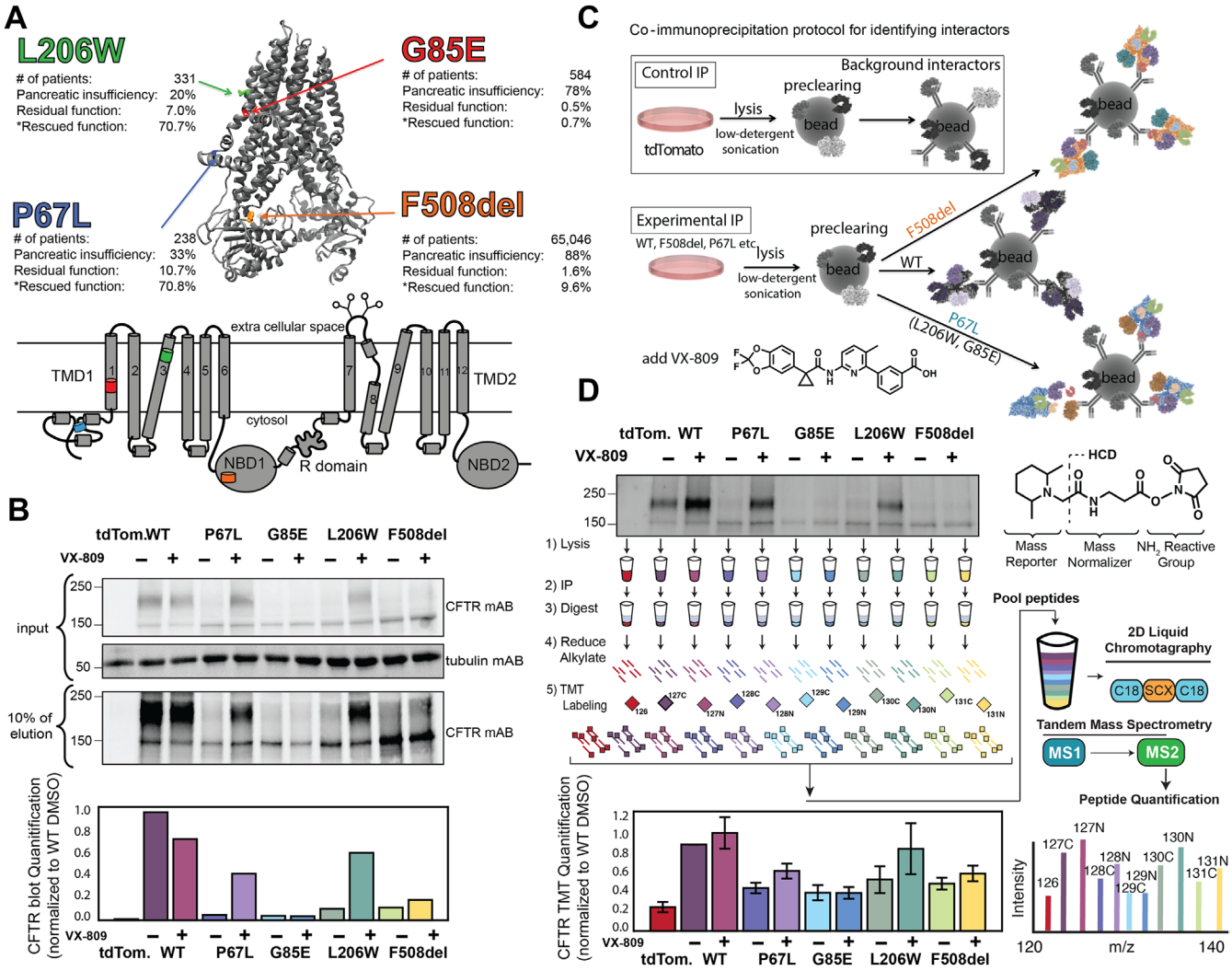

FIGURE 1: Multiplexed affinity-purification MS (AP-MS) for identification of variant specific CFTR interactomes in response to VX-809. (A) Schematic showing CFTR cryo-EM structure (PDB ID: 5UAK) and location of pathological mutations and annotation of mutations by CFTR domain. Disease severity and CFTR function in response to modulators are indicated (Han *et al.*, 2018). (B) Western blots showing expression and IP of CFTR variants in the absence or presence of 3 μM VX-809. Input from total cell lysate is shown on top. Samples were precleared with Protein G beads inputs purified on beads complexed to 24-1 CFTR antibodies. IP elution are shown at the bottom and the quantification of CFTR levels in the IP is shown normalized to the WT DMSO condition. Identification of nonspecific interactors used mock (non-CFTR expressing) cells (Pankow *et al.*, 2016). (C) Schematic of the IP procedure highlighting use of mock control and CFTR variants. Interactors likely change depending on the VX-809 response of each variant. (D) Schematic of TMT-quantification AP-MS interactomics workflow and example of multiplexed analysis of mutations and treatments to measure interactomics changes. VX-809 treated and untreated samples of WT, P67L, F508del, L206W, and G85E CFTR, as well as a tdTomato (mock) control were purified via IP. Samples are digested, and peptides are labeled with individual TMT reagents and pooled for tandem MS analysis. Relative quantification of CFTR levels recapitulates biochemical detection via Western blot (see Supplemental Figure S2 for variability in CFTR levels between replicates).

four CFTR variants and relative amounts of bands B and C were consistent with the protein levels observed in lysates (Figure 1B). As expected, we observed lower band C amounts for all the mutant variants (F508del, P67L, L206W, and G85E) compared with WT consistent with their protein trafficking defect. Importantly, we saw near restoration of band C levels for P67L and L206W with VX-809 treatment (*hyperresponders*), while F508del and G85E showed minimal to no band C in the presence of VX-809 (*moderate* and *nonresponders*) (Figure 1B). After cleanup and proteolytic digestion, we then labeled different Co-IP conditions with respective TMT 11-plex reagents (WT and 4 mutants, each ± VX-809, and mock transfection). We included a tdTomato mock transfection control to account for nonspecific background during the Co-IP to distinguish CFTR-specific interactors. After TMT labeling, combinations of 11 distinct Co-IP conditions were pooled into a single MS sample and analyzed by multidimensional protein identification technology (MudPIT)-tandem MS. In addition to peptide identification, TMT reporter ions produced during peptide fragmentation enable direct, relative comparison of peptide abundances across the different Co-IP conditions (Figure 1D). We conducted Co-IPs and independent MS runs for multiple replicates per mutation (WT $N = 10$, P67L $N = 12$, F508del $N = 11$, G85E $N = 7$, L206W $N = 7$) (Supplemental Dataset

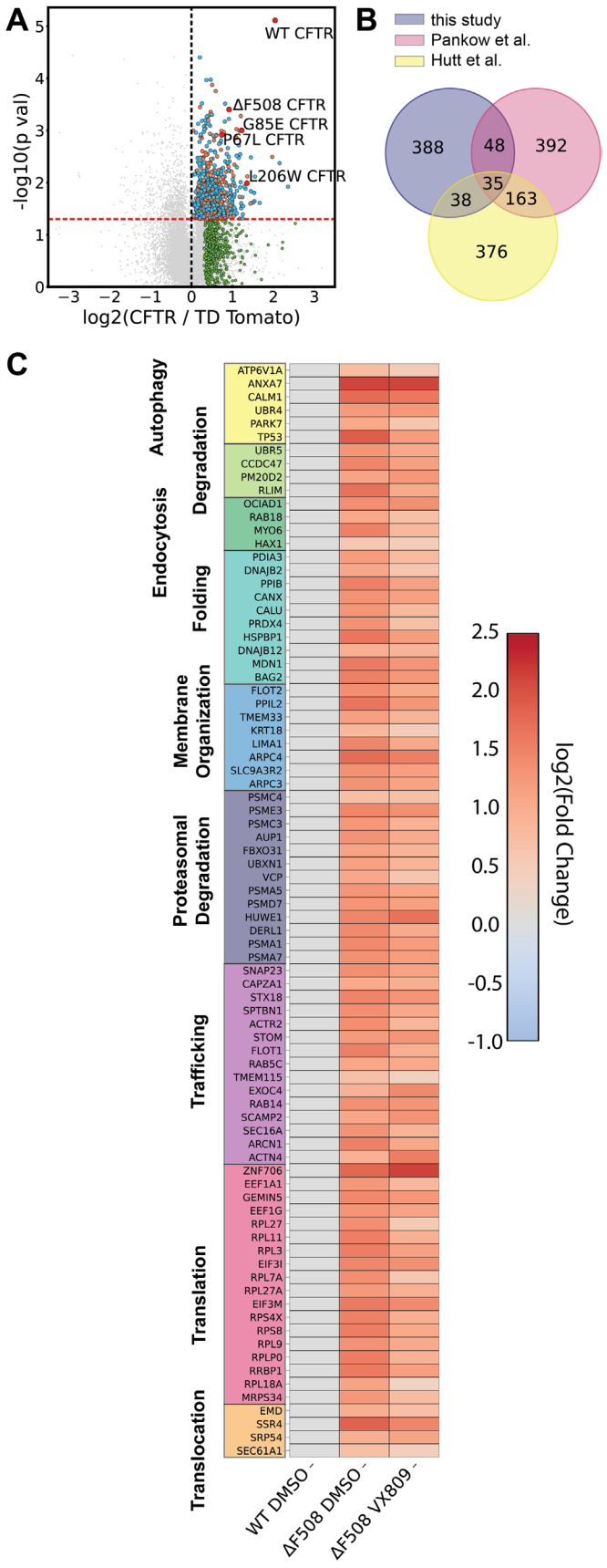

FIGURE 2: Identification and validation of altered F508del interactome with VX-809. (A) Volcano plotting showing identification of CFTR variant interactors using multiplexed AP-MS proteomics. The *x*-axis represents log2-fold change of CFTR IP over IP of tdTomato mock control. A statistical significance cutoff of $p > 0.05$ is portrayed by an orange line. Blue dots represent newly identified statistically significant interactors in this study, orange dots represent overlap with previously identified interactors from Pankow *et al.* (2015) and Hutt *et al.* (2018) that meet our statistical threshold for interactors, and green dots represent previously identified interactors (Pankow *et al.*, 2015; Hutt *et al.*, 2018) that did not meet our statistical threshold but were enriched greater than one SD of the log2-fold change distribution between CFTR over tdTomato control. (B) Overlap between statistically significant interactors identified in this study across variants considered with previously identified interactors from Pankow *et al.* (2015) and Hutt *et al.* (2018). (C) Heatmap displaying interaction changes experienced by F508del CFTR under 3 μM VX-809 treatment compared with DMSO treatment. The log2-fold changes are scaled to WT with DMSO. Proteins were selected from manually curated list of proteostasis interactors and pathways were assigned with GO-terms.

1). We used these data to validate the TMT labeling scheme applicability to CFTR interactomics and to quantitively compare interactomes of *hyper-*, *moderate-*, and *nonresponsive* mutants in response to VX-809.

Validation of TMT-based AP-MS proteomics to confirm WT and F508del CFTR interactors

Prior CFTR interactomics approaches have relied on cointeracting protein identification technology (CoPIT) with label-free quantifications (Pankow *et al.*, 2015; Hutt *et al.*, 2018; Santos *et al.*, 2019). To validate our TMT-based quantification approach, we compared our identified interactions to previous WT and F508del CFTR studies. We determined statistically significant interactors by comparing the log2 TMT intensities of identified proteins in the CFTR Co-IP samples to tdTomato mock transfected samples (Figure 2A; Supplemental Figure S1). In line with prior studies, we used median normalized TMT intensity for this comparison based on the assumption that the majority of identified proteins represent nonspecific interactors that are present in similar amounts in the mock and CFTR-bait Co-IP samples (Supplemental Figure S1A; see *Materials and Methods*) (Davies *et al.*, 2020; Wright *et al.*, 2021). WT and F508del CFTR demonstrated significant enrichment compared with tdTomato control (Supplemental Figure S1, B–E). We defined statistically significant interactors as proteins using a combined *p* value cutoff of 0.05 and a positive log2-fold change compared with tdTomato control. Our initial goal was to prioritize a comprehensive list of interactors that showed significant enrichment with any of the variants in our datasets (WT, F508del, P67L, or L206W). We compiled a list of enriched proteins for each of the individual comparisons to mock into a master list for quantitative comparison (Figure 2A; Supplemental Dataset 2). For validation, we compared the variant-specific interactor lists and the master list to prior CFTR interactome datasets.

We identified a total of 509 CFTR interactors with WT, F508del, P67L, L206W, and G85E CFTR with DMSO and VX-809 treatment conditions. Our CFTR interactome shares 83 and 73 interactors with prior datasets published by Pankow *et al.* and Hutt *et al.*, respectively (Figure 2B) (Pankow *et al.*, 2015; Hutt *et al.*, 2018). It is noteworthy that the overlap between the two prior datasets is relatively low (only ~18.8%). Some difference in identified interactors may be attributed to the use of different cell lines between our study and previous work. Our degree of overlap with both datasets is comparable with ~20% of identified interactors found in either study.

Nonetheless, we identify slightly fewer interactors in total compared with label-free proteomics studies. To understand the

limitations of our approach, we also mapped previously identified interactors on volcano plots (shown in green in Figure 2A; Supplemental Figure S1, B–E). Several prior interactors were enriched in the CFTR-bait samples compared with the mock but did not pass our statistical confidence cutoffs. We also observed other prior interactors that were enriched inconsistently in our samples. Overall, the discrepancies may result from differences in the quantification approach and higher variance in our multistep TMT sample processing procedure. At the same time, we cannot exclude the possibility that the prior label-free datasets suffered from a high false-positive discovery rate, which would explain the large number of interactors only observed in a single dataset (Figure 2B). Regardless, it is important to highlight that we consistently identified core proteostasis interactors with known function in CFTR biogenesis and trafficking (e.g., calnexin [CANX], SEC61A1, and MYO6) (Supplemental Table S1), validating our TMT-based quantitative AP-MS approach to characterize the CFTR proteostasis interactome.

We next used our master list of CFTR interactors (Supplemental Dataset 2) for subsequent quantitative comparison between CFTR variants and drug treatment conditions. We also included proteins that Pankow *et al.* (2015) and Hutt *et al.* (2018) previously identified as significant CFTR interactors that we identified as enriched greater than 1 SD of log2-fold change distribution relative to our mock control (green dots in Figure 2A; Supplemental Figure S1). We categorized our grouped list of interactors by biological pathways and refined the classifications manually using the gene ontology (GO)-terms for biological processes (see *Materials and Methods*) (Figure 2C; Supplemental Dataset 2). This analysis further highlighted that our TMT-based quantitative interactomics analysis is able to recapitulate the broad categories of CFTR proteostasis pathways identified in previous studies (Pankow *et al.*, 2015; Hutt *et al.*, 2018).

Quantitative comparison of F508del CFTR to confirm increased PN interactions

To further validate our TMT approach, we compared interaction levels between WT and F508del in the presence and absence of VX-809. Importantly, direct quantitative comparison requires normalization to the bait protein (CFTR) to account for the inherently lower CFTR levels in F508del Co-IP samples compared with WT (Figure 1B; Supplemental Figure S2; see *Materials and Methods*). We scaled the log2-fold abundances to WT DMSO condition within each run to provide a common reference point and plotted the resulting normalized interaction abundances as a heatmap organized by proteostasis pathways. We included autophagy, nonspecific degradation, endocytosis, folding, membrane organization, proteasomal degradation, trafficking, translation, and translocation (Figure 2C) as proteostasis pathways of interest. Consistent with previous findings, this heatmap reveals an overall increase in proteostasis interactions with F508del compared with WT.

F508del interacts more than WT with previously characterized proteostasis factors, such as PARK7, BAG2, DNAJB12, HSPBP1, DNAJB2, Derlin1 (DERL1), and Calnexin (CANX) (Figure 2C). Previous studies showed F508del rescue through knockdown of PARK7 (Hutt *et al.*, 2018), BAG2 (Arndt *et al.*, 2005), DNAJB12 (Grove *et al.*, 2011), and DERL1 (Sun *et al.*, 2006) or decreasing CFTR levels with coexpression of DNAJB2 (Westhoff *et al.*, 2005), indicating a prodegradation role for these proteostasis factors. By contrast, other studies show F508del rescue through overexpression of CANX (Farinha and Amaral, 2005) and HSPBP1 (Alberti *et al.*, 2004), highlighting their profolding role. Consequently, our TMT quantification approach can recapitulate the enhanced interactions with these well-characterized F508del interactors. We also find that F508del interacts more with trafficking machinery (Figure 2C), which is consistent with previous studies (Pankow *et al.*, 2015). This could reflect increased F508del dwell time with endoplasmic reticulum (ER) trafficking machinery as the protein is unable to fully translocate to the plasma membrane. Finally, F508del interacts more strongly with translation and translocation machinery (Figure 2C), likely due to increased F508del retention in the ER, slower translation (Oliver *et al.*, 2019), and membrane insertion (Rosser *et al.*, 2008).

Next, we examined how VX-809 treatment alters the proteostasis interactions for F508del. The scaled log2 TMT abundances in our multiplexed experimental setup allow for direct comparison of interaction intensities (Figure 2C). Overall, VX-809 mildly reduces interaction with proteostasis factors compared with untreated F508del. However, interactions are still broadly increased relative to WT CFTR (Figure 2C). This observation is consistent with prior interactomics characterization of the F508del response to VX-809 by Hutt *et al.* (2018), and it is likely reflective of the incomplete rescue of F508del trafficking by the corrector drug. Furthermore, Pankow *et al.* observed reduced F508del interactions with proteostasis factors on shift to low temperature (30°C), which was able to restore mutant CFTR trafficking (Pankow *et al.*, 2015). Similarly, we observed that VX-809 slightly reduces F508del interactions with folding machinery. Last, we saw some attenuation in interactions with known proteostasis factors that limit F508del trafficking, for example, BAG2 and PARK7 (Arndt *et al.*, 2005; Hutt *et al.*, 2018). Thus VX-809 reduction of F508del interaction with BAG2 and PARK7 is consistent with VX-809 correcting F508del folding sufficiently to attenuate these prodegradation interactions. We also examined WT CFTR interaction changes in the presence of VX-809 and found that several proteostasis interactions are reduced (Supplemental Figure S3A). The overall identification of these important proteostasis components and quantification of their down-regulation with VX-809 supports our ability to measure subtle protein interaction changes with TMT labeling. With our approach validated, we then examined protein interaction changes for the *hyper-*, *moderate-*, and *nonresponsive* CFTR variants.

Class-II misfolding mutation P67L exhibits similar interactome to F508del

We first examined the class-II variant P67L, which is much more responsive to VX-809 treatment than F508del, exhibiting restoration of band C CFTR levels similar to WT (Figure 1B). The P67L mutation occurs in the lasso-motif helix-helix bend at the CFTR N-terminus (Figure 1A). The mutation prevents proper N-terminal/C-terminal interactions resulting in ER retention and premature degradation (Sabusap *et al.*, 2021). Our previous investigations of P67L by Western blot trafficking assay, Ussing chamber electrophysiology, sequence conservation analysis, and molecular dynamics simulation characterized P67L as a VX-809 *hyperresponder* (Sabusap *et al.*, 2016; Sabusap *et al.*, 2021). However, the cellular proteostasis interactome of P67L remains unknown.

Since P67L and F508del share a similar fate in the ER as trafficking-defective mutants, we hypothesized P67L exhibits similar protein interactions to F508del compared with WT. We measured P67L interactions using TMT labeled LC-MS proteomics. Overall, we identified 86 statistically significant P67L interactors when comparing the enrichment to the mock control (Figure 3A). Similarly to F508del, we found up-regulated interactors included proteostasis factors such as calnexin (CANX), calmodulin (CALM1), Sec61A, and BAG2 (Figure 3A).

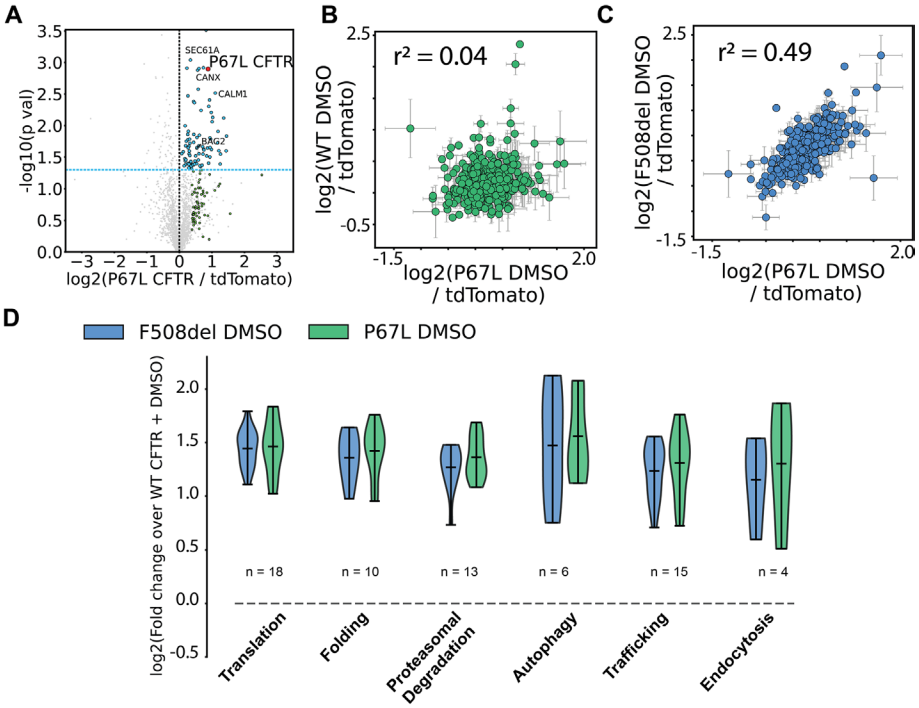

FIGURE 3: Newly identified P67L interactome correlates with class-II misfolding variant F508del interactome. (A) Identification of P67L CFTR interactors using multiplexed AP-MS proteomics. The *x*-axis represents log2-fold change of CFTR IP over IP of tdTomato mock control. A statistical significance cutoff of $p > 0.05$ is portrayed by a dotted blue line. Blue dots represent newly identified statistically significant interactors in this study and green dots represent previously identified interactors from Pankow *et al.* (2015) and Hutt *et al.* (2018) that did not meet our statistical cutoff threshold but were enriched greater than 1 SD of the log2-fold change distribution between CFTR vs. tdTomato control. (B) Correlation between quantified protein interactors of P67L with DMSO and WT with DMSO. Specific interactions plotted were identified by us or Pankow *et al.* (2015) and Hutt *et al.* (2018) in our master list. The R value represents the Pearson correlation coefficient. (C) Correlation between P67L and DMSO and F508del and DMSO among specific interactions identified by us and others in our master list. (D) Violin plots comparing the aggregate protein enrichments with important proteostasis pathways for F508del or P67L CFTR. All log2-fold changes are scaled to WT treated with DMSO. Pathways were assigned with GO-terms, categorized based on previous pathway characterization by Pankow *et al.* (2015), and further refined manually. These plots demonstrate up-regulated interactions with important proteostasis in the class-II variants compared with WT; *n* represents the number of identified proteins in the considered pathway (Supplemental Dataset 4). No statistically significant difference between F508del and P67L was detected for these pathways.

We correlated the interaction fold changes for the class-II variants across all proteins in our master list. Interaction fold changes do not correlate between P67L and WT (Pearson correlation coefficient $r^2 = 0.04$) (Figure 3B). By contrast, the interaction fold changes correlate well between P67L and F508del ($r^2 = 0.49$) (Figure 3C). This is consistent with previous findings that class-II variant interactors correlate better with each other than with WT CFTR (Hutt *et al.*, 2018). Furthermore, P67L shares more interactors with F508del than with WT (Supplemental Figure S4A). Thus the class-II mutants demonstrate greater overlap with one another than they share with WT. Together these data confirm our hypothesis that the P67L interactome resembles F508del.

Next, we compared the interaction fold changes between F508del and P67L for specific proteostasis pathways with known roles in CFTR processing. For this purpose, we plotted for each pathway the distributions of log2-fold interaction changes for F508del and P67L CFTR scaled to WT (Figure 3D). Consistent with the global correlations, both F508del and P67L showed increased interactions with all pathways included in the analysis. P67L demonstrated no substantial differences from F508del in these aggregated interactions. In line with their class-II misfolding categorization, P67L and F508del associated on average more with translational proteins, folding machinery, degradation pathways, and trafficking factors compared with WT (Figure 3D). Both mutants also associate more with endocytosis proteins consistent with CFTR quality control at the plasma membrane (Okiyoneda *et al.*, 2010) (Figure 3D). Notably, pathways important for CFTR biogenesis, such as folding, show a shaper distribution of log2-fold change compared with pathways less clearly associated with CFTR biogenesis (Supplemental Figure S4, B and C). Together, these data demonstrate that P67L and F508del share similar increased interactions with important proteostasis pathways.

VX-809 produces an inflection point in P67L interactions between folding and degradation

We next sought to determine how the corrector VX-809 remodels the PN of P67L CFTR. Specifically, we compared these alterations to F508del to better understand how the PN influences the *hyperresponsiveness* and trafficking restoration of P67L to the corrector drug. We identified 104 P67L interactors under VX-809 treatment when normalized to tdTomato control (Figure 4A). These included previously identified proteostasis factors important for CFTR processing such as BAG2, CANX, and CALM1 (Figure 4A). Of our identified interactors, 27 of these interactors overlapped with P67L with DMSO and 14 interactors overlapped with WT (Supplemental Figure S4D).

Next, we quantitatively compared protein levels of P67L interactors between DMSO and VX-809 conditions at the pathway level (Figure 4B). The heatmap confirmed the overall reduction in P67L interactors when treated with VX-809. Specifically, VX-809 reduced P67L interaction with CANX, BAG2, HSPBP1, DNAJB12, DERL1, various proteasomal subunits (PSMA1, PSMA5, PSMA7, PSMC3, PSMC4, and PSME3), as well as eukaryotic initiation factors and ribosomal proteins (Figure 4B).

To gain insights into how specific proteostasis pathways are impacted by VX-809, we considered the aggregate distribution of interaction changes for individual pathways (Figure 4C). We plotted pathway changes in approximate order of biogenesis: translation, folding, proteasomal degradation, autophagy, trafficking, and endocytosis with the caveat that many of these processes are known to occur simultaneously (Du *et al.*, 2005; Kleizen *et al.*, 2005). VX-809 significantly reduced both F508del and P67L interactions with folding and translational machinery with a similar mean change (Figure 4C). Considering later pathways, VX-809 reduced P67L interactions more than F508del interactions with proteasomal degradation and autophagy machinery (Figure 4C). Yet downstream pathways such

as trafficking and endocytosis are only reduced by VX-809 in P67L and not F508del. These data suggest VX-809 produces an inflection point in P67L proteostasis interactions between folding and proteasomal degradation/autophagy (Figure 4C). By contrast, VX-809 does not show this inflection point for F508del proteostasis interactions.

Thus distinct proteostasis alterations emerge when comparing *moderate-responsive* and *hyperresponsive variants*: *the moderate-responsive* F508del continues to experience greater proteasomal and autophagy degradation under VX-809 treatment while these pathways are attenuated for P67L (Figure 4C). Subsequent pathways such as trafficking and endocytosis also have reduced P67L interactions when treated with VX-809.

To determine which specific proteasomal interactions are reduced by VX-809, we plotted the correlation of interaction fold changes for proteasomal interactors between DMSO versus VX-809 treatment. We examined these correlations separately for F508del and P67L and fitted each correlation using a linear regression (Figure 4, D and E). F508del proteasomal interactors remain close to the normal line (black dotted line), implying good correlation between DMSO and VX-809 conditions (Figure 4D). On the other hand, P67L proteasomal interactors fall below the normal line, implying they are reduced in the VX-809 condition (Figure 4E). VX-809 reduces PSMC3 and PSMC4 interactions the most as they fall the furthest beneath the normal line (Figure 4E).

Next, to determine specific autophagy interactions reduced by VX-809, we plotted the same correlation for these proteins (Figure 4F-G). Again, F508del autophagy interactors remain close to the normal line, implying good correlation between DMSO and VX-809 conditions (Figure 4F). By contrast, P67L autophagy interactors are globally reduced by VX-809 treatment (Figure 4G). In particular, VX-809 reduces P67L interactions with ANXA7, a GTPase with a regulatory role for autophagy (Xi *et al.*, 2020) (Figure 4G). These analyses highlight other potential protein targets for CF treatment in less responsive mutants. We also compared correlations for translation and folding proteins (Supplemental Figure S4, E and F). These plots reveal further interactions of P67L that are greatly attenuated with VX-809 treatment, such as DNAJB12 in the folding correlations (Supplemental Figure S4F). Together, these data highlight that VX-809 alters specific proteostasis interactions for P67L compared with F508del that may be associated with the *hyperresponse* to the corrector.

To further support our model that VX-809 creates an inflection point for P67L but not for F508del, we validated interaction levels for key folding and degradation proteins by Co-IP followed by Western blot. Well-characterized CFTR interactors BAG2, Derlin-1, and CANX were chosen for their known role in folding and degradation (Arndt *et al.*, 2005; Farinha and Amaral, 2005; Sun *et al.*, 2006). We also monitored PSMC3, whose interactions with P67L was more strongly reduced by VX-809 than with F508del (Figure 4E). Consistent with our interactomics data, VX-809 significantly reduced P67L interaction with BAG2, Derlin-1, CANX, and PSMC3 (Supplemental Figure 5). By contrast, VX-809 failed to reduce F508del interaction with these proteins (Supplemental Figure S5).

In summary, our data show commonalities in the way that VX-809 treatment attenuates the proteostasis interactions of both F508del and P67L, reducing interactions with folding and translation proteins. At the same time, distinct interaction changes between the two mutants point to routes by which VX-809 treatment can better restore P67L plasma membrane trafficking. Our data indicate that resetting of degradation interactions may produce an inflection point in the *hyperresponsiveness* for P67L as these pathways are shifted closer to WT levels for P67L than for F508del (Figure 4C). Subsequently, P67L also experiences reduced interactions with trafficking machinery under VX-809 treatment, which could indicate faster flux through the pathway.

L206W and G85E CFTR interactomics reveal pathway commonalities between hyperresponsive and nonresponsive variants

To further understand how VX-809 treatment generally affects CFTR interactions, we turned to another *hyperresponsive* mutation, L206W, as well as the *nonresponsive* mutant G85E. L206W is an N-terminal class-II CFTR variant associated with mild CF disease (Rozen *et al.*, 1995) (Figure 1A). L206W impairs CFTR biosynthesis, typical of class-II variants, but demonstrates single-channel conductance similar to WT CFTR (Clain *et al.*, 2005), indicating that plasma membrane-localized L206W retains some function. Second, we chose G85E, an N-terminal class-II variant that cannot be corrected by VX-809 (Okiyoneda *et al.*, 2013) (Figure 1A).

L206W CFTR exhibited near WT levels of band C when treated with VX-809, confirming a *hyperresponse* like P67L (Figure 5A). On the other hand, very minimal band C CFTR was observed for the G85E variant regardless of VX-809 addition (Figure 5B). We measured L206W and G85E CFTR protein interactions with TMT labeled LC-MS/MS to understand what common and distinct interaction changes occur with VX-809 treatment for the *hyper-* and *moderate-* or *nonresponsive* variants. Importantly, several of the TMT11plex sets included conditions for WT CFTR and all four variants (± VX-809) allowing for direct comparison of the interaction fold changes in the integrated dataset (Supplemental Dataset 1).

We first defined statistically significant interactors of the individual L206W and G85E variants. A previous proteomics dataset has been published on G85E for comparison (Hutt *et al.*, 2018) (Supplemental Figure S6). We identified 86 statistically significant L206W interactors under DMSO and 66 interactors under VX-809 treatment (Supplemental Figure S6, A and B). P67L and L206W interactors correlate moderately for proteins early in biogenesis such as translation, folding, and degradation, and correlation increases for later pathways such as trafficking and endocytosis regardless of DMSO or VX-809 treatment (Supplemental Figure S7, A–F). We also identified 206 statistically significant G85E interactors under DMSO and 146 interactors under VX-809 treatment (Supplemental Figure S6, C and D), consistent with an increased number of interactions with *nonresponsive* variants seen in a previous published study (Pankow *et al.*, 2015). From our dataset, 32 G85E interactors overlapped with the previous G85E datasets, albeit the general overlap was relatively small (11.6% interactors among protein we identified) (Supplemental Figure S6E).

Next, we compared the interaction fold changes between CFTR variants under VX-809 treatment conditions (Figure 5C). As with the prior class-II CFTR mutant, we observed overall increases in proteostasis interactions with L206W and G85E compared with WT when treated with DMSO. This is consistent with the enhanced proteostasis surveillance experienced by these destabilized, trafficking-defective mutants. The overall magnitude of the increase is lower for L206W DMSO than for G85E DMSO (Figure 5C), which could reflect the milder trafficking defect of L206W. We then examined how VX-809 treatment restores the proteostasis interactions. The data clearly highlighted the global decrease in interactions for L206W under VX-809 treatment. By contrast, G85E demonstrated little change in the presence of the corrector.

To gain deeper insight into the impact of VX-809 treatment on distinct proteostasis pathways, we plotted the interaction

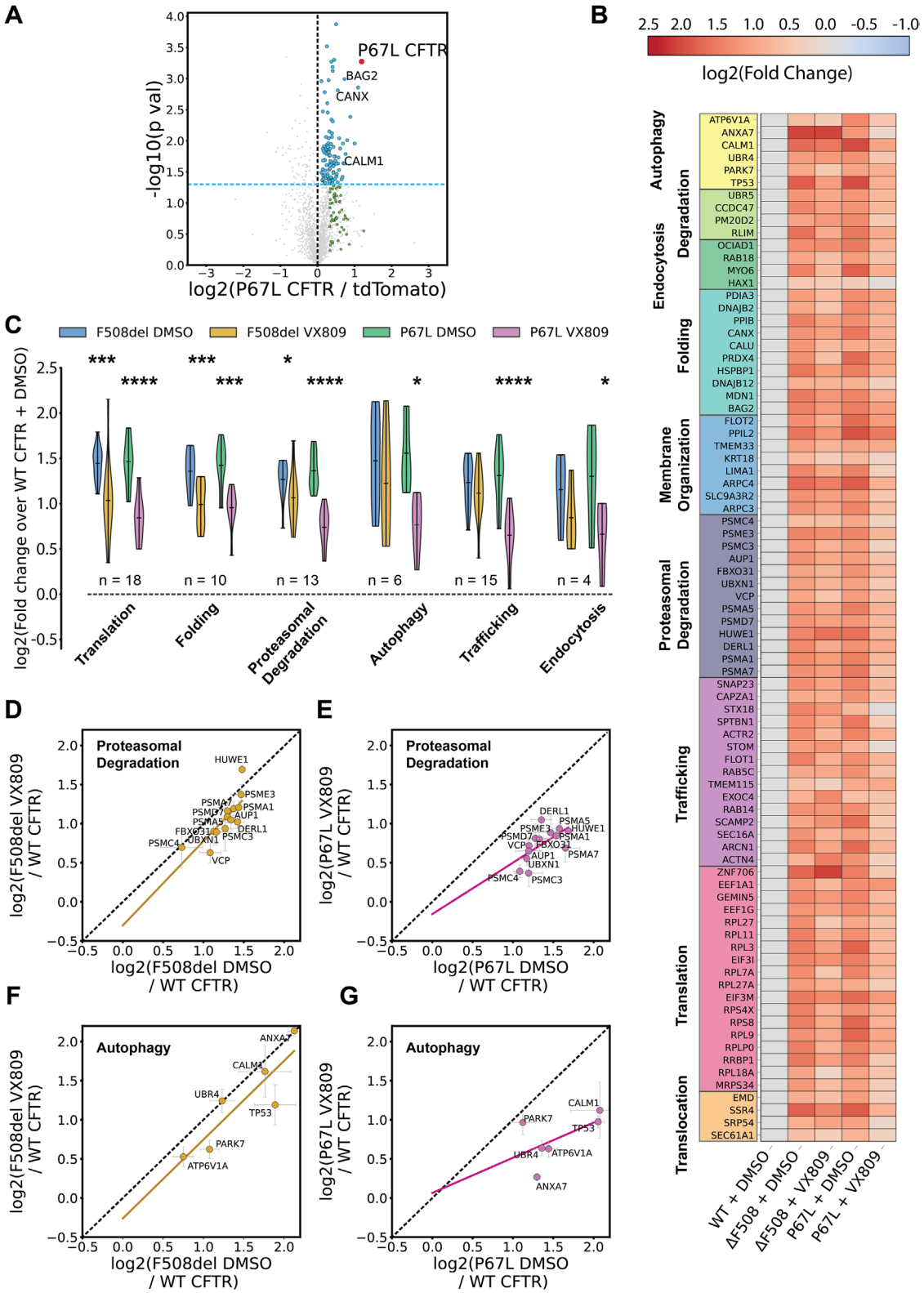

FIGURE 4: Comparison of *hyperresponsive* P67L and *moderate-responsive* F508del interactomes reveals VX-809 produces at an inflection point of CFTR interactions between folding and degradation. (A) Identification of P67L interactors with 3 μM VX-809 treatment using multiplexed AP-MS proteomics. The *x*-axis represents log2-fold change of CFTR IP over IP of tdTomato mock control. A statistical significance cutoff of $p > 0.05$ is portrayed by a blue dotted line. Blue dots represent newly identified statistically significant interactors in this study and green dots represent previously identified interactors that did not meet our statistical cutoff threshold but were enriched greater than one SD of the log2-fold change distribution between CFTR vs. tdTomato control. (B) A pathway ordered heatmap comparing F508del and P67L interactions under DMSO and VX-809 conditions. Log2-fold changes are scaled to WT with DMSO. Proteins

abundance changes grouped by pathways under the various conditions (Figure 5D). Like P67L, L206W experienced significantly decreased interactions with translational, folding, proteasomal degradation, autophagy, and trafficking pathways. On the other hand, G85E did not show a significant change in any pathway interactions in the presence of VX-809, which reflects its classification as a *nonresponsive* variant (Figure 5D). Together, these data highlight that pathway analysis of interaction changes for CFTR variants under VX-809 treatment can clearly distinguish *hyperresponsive* and *nonresponsive* CFTR variants.

To elucidate specific proteasomal interactions reduced by VX-809, we plotted the correlation of interaction fold changes for proteasomal interactors with DMSO versus VX-809 treatment for L206W. We compared this correlation with G85E (Figure 5, E and F). Linear regression best fit reveals L206W proteasomal interactions fall below the normal line, implying VX-809 reduces these interactions (Figure 5E). VX-809 globally reduces L206W interactions with proteasomal proteins and reveals few outliers (Figure 5E). By contrast, G85E proteasomal interactions straddle the normal line, implying VX-809 does not affect these interactions (Figure 5F). Likewise, L206W autophagy interactions fall below the normal implying reduction by VX-809 (Figure 5G), whereas G85E interactions remain unaffected (Figure 5H). Furthermore, L206W interactions fall below the normal line for translational, folding, and trafficking proteins, whereas G85E interactions correlate close to the normal line (Supplemental Figure S8).

Overall, the data shows that *hyperresponsive* variants, such as P67L and L206W, display global attenuation of proteostasis interactions closer to WT levels, in particular reduced interactions with proteasomal degradation and autophagy pathways. In contrast, *moderate or nonresponsive* variants maintain prolonged interactions with translation machinery and are not rescued from engagement with degradation machinery by VX-809 treatment. An interesting distinction between the *moderate* and the *nonresponsive* variants is that F508del displays some reductions in proteostasis interactions with folding and translation components when treated with VX-809 (Figure 4C), while G85E interactions are completely refractory to the corrector compound (Figure 5D) (Van Goor *et al*., 2011).

Measuring the interactions of distinct drug responsive variants reveals the defining characteristics of *hyperresponsive* mutations, or theratype. The ability of VX-809 to attenuate interactions with translational, folding, and proteasomal degradation components in responsive CFTR variants appears to be critical to this pharmacological chaperone theratype.

Inhibiting proteasomal degradation and autophagy differentially impacts the VX-809 rescue of hyperresponders and moderate responders

We demonstrated VX-809 likely produces an inflection point in proteasomal and autophagy interactors for *hyperresponsive* CFTR variants P67L and L206W. For this reason, we chose to further investigate how proteasomal and autophagy degradation pathways contribute to the divergent VX-809 correction levels experienced by the *hyper-, moderate, and nonresponsive* CFTR variants. F508del is a well-known target of ER-associated degradation (ERAD) which directs the protein to the proteasome (Loo *et al*., 1998). Inhibition of ERAD by proteosome inhibitors such as bortezomib (Paramore and Frantz, 2003) is known to partially rescue F508del CFTR (Farinha and Amaral, 2005).

To test the impact of proteasome inhibition on VX-809 rescue, cells expressing mutant CFTR variants were cotreated with VX-809 and bortezomib. Subsequent effects on CFTR expression and trafficking were analyzed by Western blot. Consistent with prior studies, bortezomib treatment alone resulted in a strong buildup of immature F508del CFTR and threefold increase in mature CFTR (Figure 6, A and B; Supplemental Figure S9A) (Farinha and Amaral, 2005). This increase was slightly higher than with VX-809 treatment alone. We also quantified trafficking efficiency by considering the ratio of band C band relative to total CFTR (band C/[band B + band C]) (Supplemental Figure S9B). We then compared how bortezomib treatment affects the VX-809 response for F508del. Cotreatment resulted in higher band C F508del amounts compared with bortezomib or VX-809 treatment alone (Figure 6, A and B) and trafficking efficiency continued to increase in response to VX-809 (Supplemental Figure S9B). These data indicated that proteasome inhibition still allows for further F508del VX-809 correction.

We then probed the impact of proteasome inhibition on P67L CFTR. Bortezomib treatment resulted in strong band B P67L accumulation but in contrast to F508del did not increase band C P67L CFTR (Figure 6, C and D; Supplemental Figure S9C). This suggests that the accumulated immature P67L population fails to traffic. We then tested whether VX-809 could restore P67L trafficking in the presence of proteasome inhibition. Surprisingly, cotreatment of bortezomib and VX-809 abrogated P67L band C accumulation (Figure 6, C and D), indicating that the proteasome inhibitor interferes with VX-809 correction. Similarly, cotreatment of bortezomib and VX-809 reduced trafficking efficiency compared with VX-909 treatment alone (Supplemental Figure S9D).

were selected from manually curated list of proteostasis interactors and pathways were assigned with GO-terms. (C) Violin plots comparing the aggregate protein enrichment levels of important proteostasis pathways for F508del and P67L in the presence and absence of VX-809 treatment (3 μM). Pathways were assigned with GO-terms and annotated manually or by searching previous pathway characterization by Pankow *et al*. (2015). Violin plots reveal 3 μM VX-809 produces an inflection point in P67L interactions between proteasomal degradation and autophagy, as these pathways are not as reduced in F508del; *n* represents the number of identified proteins in the considered pathway (Supplemental Dataset 4). Statistical significance calculated by one-way ANOVA with Geisser-Greenhouse correction and Tukey post-hoc multihypothesis correction. Adjusted *p* values depicted by *< 0.05, **< 0.01, ***< 0.001, and ****< 0.0001. (D) Proteasomal degradation protein quantifications correlated for F508del between DMSO and 3 μM VX-809 treatment (all log2-fold changes normalized to WT with DMSO). The black dotted line represents the normal line with a slope of 1 and intercept at the origin. The gold dotted line is the linear least-squared best fit for the proteasomal proteins. (E) Proteasomal degradation protein quantifications correlated for P67L between DMSO and 3 μM VX-809 treatment normalized to WT with DMSO. The purple dotted line is the linear least-squared best fit of the proteasomal proteins. (F) Autophagy protein quantifications correlated for F508del between DMSO and 3 μM VX-809 treatment normalized to WT with DMSO. The gold dotted line is the linear least-squared best fit of the autophagy proteins. (G) Autophagy protein quantifications correlated for P67L between DMSO and 3 μM VX-809 treatment normalized to WT with DMSO. The purple dotted line is the linear least-squared best fit of the autophagy proteins.

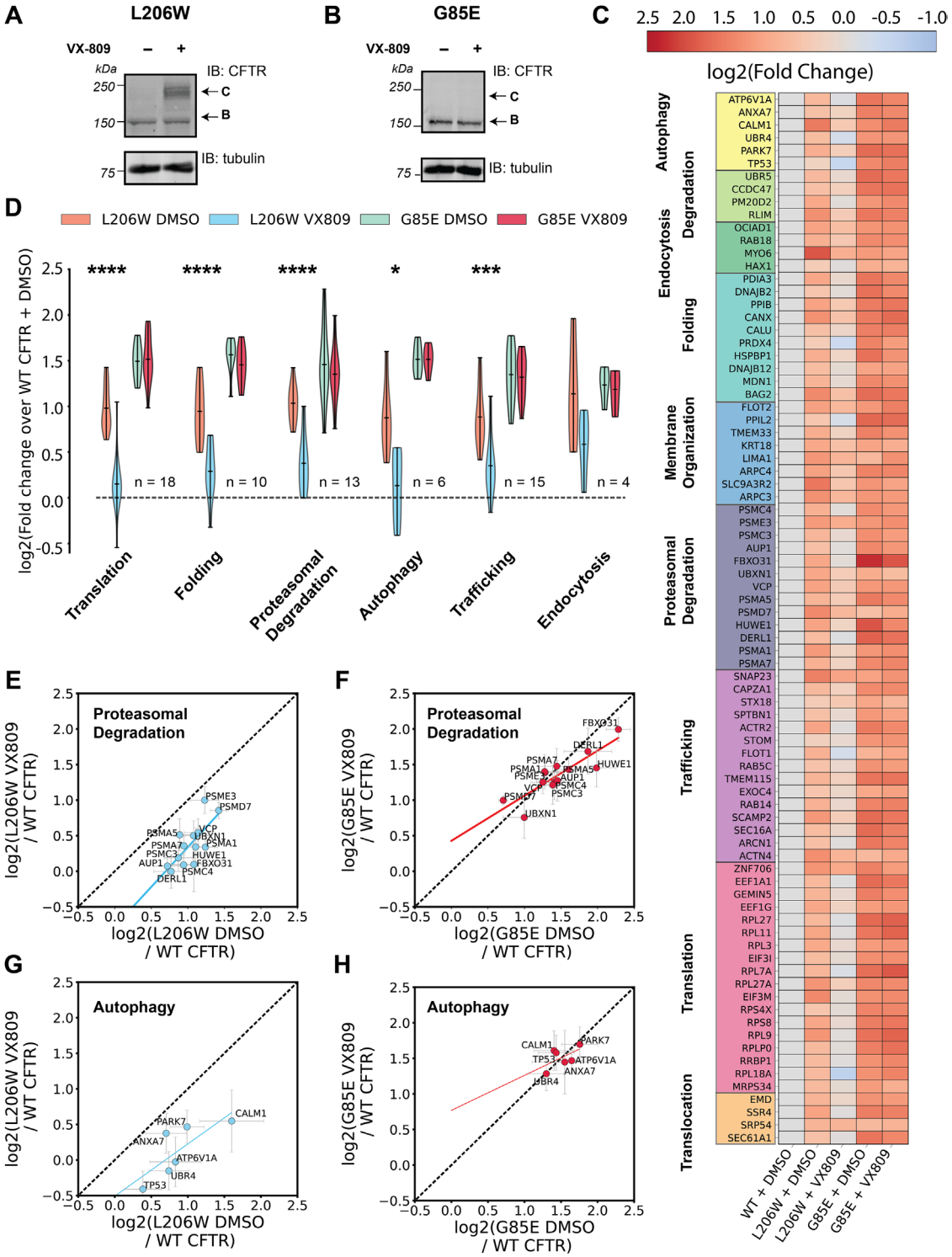

FIGURE 5: L206W interactome with VX-809 reveals similar changes in degradation pathways not observable in nonresponsive G85E. (A, B) Western blot cell lysates expressing L206W (A) or G85E (B) CFTR probed with CFTR 217 antibody and tubulin loading control. Comparison of C Band CFTR between DMSO and 3 μM VX-809 treatment demonstrates L206W classification as a *hyperresponsive* variant, while G85E is a *nonresponsive* variant. (C) A pathway ordered heatmap comparing L206W and G85E interactions under DMSO and 3 μM VX-809 conditions (all log2-fold changes scaled to WT with DMSO). Proteins were selected from manually curated list of proteostasis interactors and pathways were assigned with GO-terms. (D) Violin plots comparing aggregate protein enrichment levels for important proteostasis pathways between L206W and G85E CFTR in the presence and absence of VX-809 (3 μM). Pathways were assigned with GO-terms and annotated manually or by searching previous pathway characterization by Pankow *et al.* (2015). Violin plots reveal 3 μM VX-809 reduces L206W proteostasis interactions which are not reduced in G85E; *n* represents the number of identified proteins in the considered pathway (Supplemental Dataset 4). Statistical significance calculated by one-way ANOVA with Geisser-Greenhouse correction and Tukey post-hoc multihypothesis

Prolonged bortezomib treatment can lead to considerable remodeling of the PN, in part through activation of the unfolded protein response (Obeng *et al.*, 2006). To ensure that the divergent reduction in VX-809 response is directly attributed to proteasomal inhibition and to rule out the possibility of indirect effects, we repeated the dual treatment with VX-809 and bortezomib for shorter duration (6 h)—sufficient time to allow for CFTR buildup but not extensive translational up-regulation of proteostasis factors (Lin *et al.*, 2007). We found that this shorter treatment also abrogated the VX-809 rescue for P67L (Supplemental Figure S9, E–H). These data further suggest a previously unknown role for proteasomal degradation in VX-809 corrections.

Given the distinct impact of proteasome inhibition on P67L and F508del, we turned to examine additional degradation pathways. Autolysosomal degradation is another important pathway for removal of CFTR after targeting by ER-associated autophagy or endocytic removal CFTR from the plasma membrane (Okiyoneda *et al.*, 2010; He *et al.*, 2021). We used the cathepsin protease inhibitor E-64 to broadly block lysosomal protein degradation (Barrett *et al.*, 1982). E-64 treatment did not result in any accumulation of F508del or P67L band B or band C (Figure 6, E and F; Supplemental Figure S9, A–D), confirming that autolysosomal degradation is not critical for the clearance of these variants under corrector treatment. Cotreatment of E-64 with VX-809 failed to change the correction for P67L as assessed by similar band C levels (Figure 6, E and F) and trafficking efficiency (Supplemental Figure S9D). Similarly, E-64 did not impact the modest F508del correction afforded by VX-809 (Figure 6, E and F; Supplemental Figure S9, A and B).

The unique dependency of P67L CFTR on proteasomal degradation during VX-809 correction prompted us to examine the L206W and G85E variants. Cotreatment of inhibitors with VX-809 showed that proteasomal inhibition again impaired the correction of L206W, but autolysosomal inhibition did not (Supplemental Figure S9, I–L). Thus both *hyperresponsive* L206W and P67L variants exhibit similar dependences on active proteasomal degradation for correction by VX-809. Last, G85E exhibited a small amount of restoration of band C CFTR with bortezomib treatment regardless of VX-809 treatment (Supplemental Figure 9, M–P). Together these data suggest that autolysosomal inhibition does not affect VX-809 *hyperresponders* P67L and L206W. By contrast, our data suggest that VX-809 requires proteasomal degradation for effective correction of the *hyperresponsive* variants.

DISCUSSION

This study represents, to our knowledge, the first quantitative interactomics analyses comparing CFTR mutations with diverse VX-809 response. We used AP-MS coupled to TMT labeling, which allows sample multiplexing and direct quantitative comparison of protein interaction changes between mutants and treatments simultaneously. Prior studies from our group used this platform to explore how the ER PN facilitates protein quality control for misfolding-prone proteins, such as amyloidogenic light chains and thyroid prohormones (Plate *et al.*, 2019; Wright *et al.*, 2021). Here we extend the multiplexed, quantitative TMT-based MS platform to compare CFTR interactome changes across patient mutations F508del, P67L, L206W, and G85E, which exhibit distinct response profiles to clinically approved therapeutic correction. Comparing drug-induced interaction changes between *hyperresponsive* mutations (P67L and L206W), *moderate-responsive* mutation F508del, and *nonresponsive* G85E revealed important proteostasis components that may drive drug susceptibility. Specifically, we found *hyperresponsive* mutations to associate less with proteasomal and autophagy degradation machinery.

We first evaluated the ability of our approach to recapitulate the known proteostasis interactions of F508del CFTR. Consistent with previous findings, we show F508del interacts more with proteostasis factors than WT. We identified many novel F508del interactors as well as demonstrated comparable overlap with previous data (Pankow *et al.*, 2015; Hutt *et al.*, 2018). Importantly, our TMT-based quantification provides the ability to directly compare F508del interactions under VX-809 treatment, and although previous studies have made similar comparisons, they used label free quantification (Hutt *et al.*, 2018). We also note that use of different cell lines in this study may lead to different identified protein–protein interactions and may explain the observed low degree of overlap between ours and previous datasets. This analysis revealed that F508del interacts less with proteostasis components when treated with VX-809 similar to F508del interactome remodeling during temperature correction (Pankow *et al.*, 2015). Specifically, VX-809 reduced F508del interactions with translational, folding, and proteasomal degradation pathways. On the individual protein level, VX-809 lowered interactions with previous characterized F508del proteostasis components such as CANX, MYO6, BAG2, DNAJB12, DNAJB2, and several factors whose knockdown restores F508del trafficking. These results highlight that our TMT quantification approach can detect the drug-mediated, reduced interaction between F508del and well-validated protein quality control factors. Thus we turned to P67L to determine which protein interactions underlie *hyperresponsive* VX-809 correction.

Despite extensive characterization of P67L as a VX-809 *hyperresponsive* CFTR variant (Sabusap *et al.*, 2016; Sabusap *et al.*, 2021), its proteostasis interactome remained undefined until this study. We found increased overlap and correlation with F508del compared with WT CFTR. These overlapping proteostasis components included chaperones, degradation machinery, translation, and trafficking proteins (Figure 4A). We then quantitatively compared P67L interactions under VX-809 treatment conditions to determine which specific protein interaction changes are associated with the *hyperresponsive* behavior of P67L CFTR to the corrector drug. In the presence of VX-809, the P67L interactions shifted toward WT levels, as

correction. Adjusted *p* values depicted by *< 0.05, **< 0.01, ***< 0.001, and ****< 0.0001. (E) Proteasomal degradation protein quantifications correlated for L206W between DMSO and 3 μM VX-809 treatment normalized to WT with DMSO. The black dotted line represents a normal line with a slope of 1 and intercept at the origin. The blue dotted line is the linear least-squared best fit of the proteasomal proteins. (F) Proteasomal degradation protein quantifications correlated for G85E between DMSO and 3 μM VX-809 treatment normalized to WT with DMSO. The red dotted line is the linear least-squared best fit of the proteasomal proteins. (G) Autophagy protein quantifications correlated for L206W between DMSO and 3 μM VX-809 treatment normalized to WT with DMSO. The blue dotted line is the linear least-squared best fit of the autophagy proteins. (H) Autophagy protein quantifications correlated for G85E between DMSO and 3 μM VX-809 treatment normalized to WT with DMSO. The red dotted line is the linear least-squared best fit of the autophagy proteins.

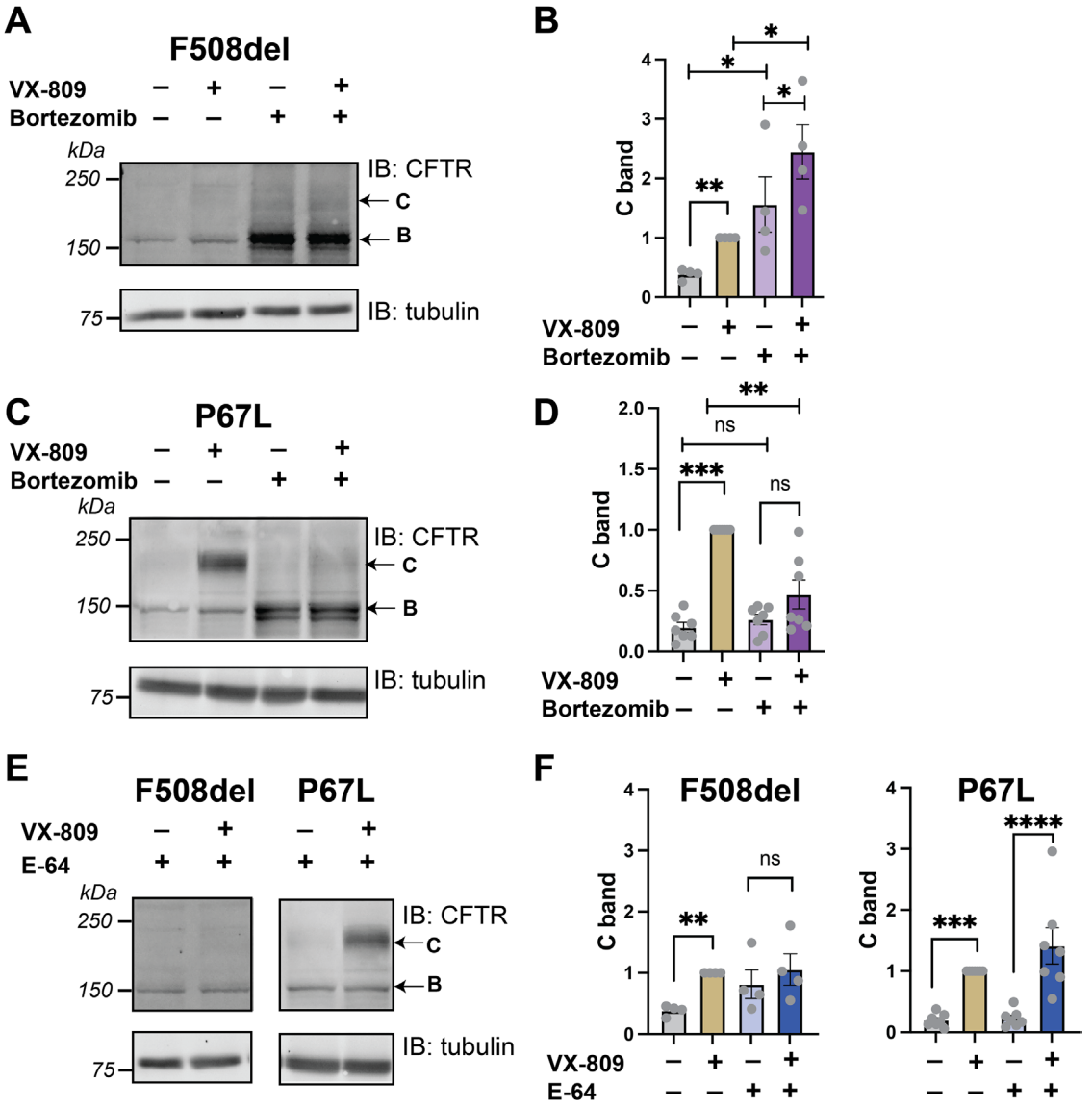

FIGURE 6: Inhibiting proteasomal degradation attenuates *hyperresponsive* P67L and L206W VX-809 response, while inhibiting lysosomal degradation attenuates *moderate-responsive* F508del VX-809 response. (A) Representative Western blot of F508del CFTR trafficking assay. Cells expressing F508del CFTR were treated with 3 μM VX-809, 10 μM bortezomib, or a combination. Cell lysates samples were separated by SDS–PAGE and blots were probed with 217 CFTR antibody and tubulin antibody as a loading control. (B) Quantification of mature (C band) F508del levels from Western blot data showing. Band C (post-Golgi) F508del CFTR levels were normalized to the 3 μM VX-809 treatment condition. (C) Representative Western blot of P67L CFTR trafficking assay. Cells expressing F508del CFTR were treated with 3 μM VX-809, 10 μM bortezomib, or a combination. Blots were probed with 217 CFTR antibody and tubulin antibody as a loading control. (D) Quantification of mature (C band) P67L Western blot data showing the relative post-Golgi P67L CFTR normalized to the 3 μM VX-809 treatment condition. (E) Representative Western blot of F508del and P67L CFTR trafficking assay when cells were treated 10 μM E-64 (cysteine protease inhibitors) or a combination of E-64 with 3 μM VX-809. Blots were probed with 217 CFTR antibody and tubulin antibody as a loading control. (F) Quantification of mature (C band) CFTR Western blot data for F508del and P67L showing the relative post-Golgi CFTR normalized to the 3 μM VX-809 treatment condition. For all graphs, individual measurements are shown as grey points, error bars represent standard error of the mean, statistical significance was calculated with a paired, two-tailed student *t* test and *p* values are depicted by *< 0.05, **< 0.01, ***< 0.001 and ****< 0.0001.

demonstrated by a broad reduction in the magnitude of interactions with proteostasis factors in the heatmap (Figure 4B).

These observations are consistent with a shift toward WT protein quality control for *hyperresponsive* mutations during correction. Commonalities for P67L and F508del CFTR are attenuated interactions with translation and folding components in the presence of VX-809. Importantly, we found that VX-809 uniquely attenuates interactions with proteasomal degradation, autophagy, trafficking, and endocytosis proteins for P67L. These interactions are maintained for F508del even in the presence of VX-809, pointing toward their distinct role in the *hyperresponsive* behavior. To determine the interaction commonalities underlying a robust VX-809 response, we

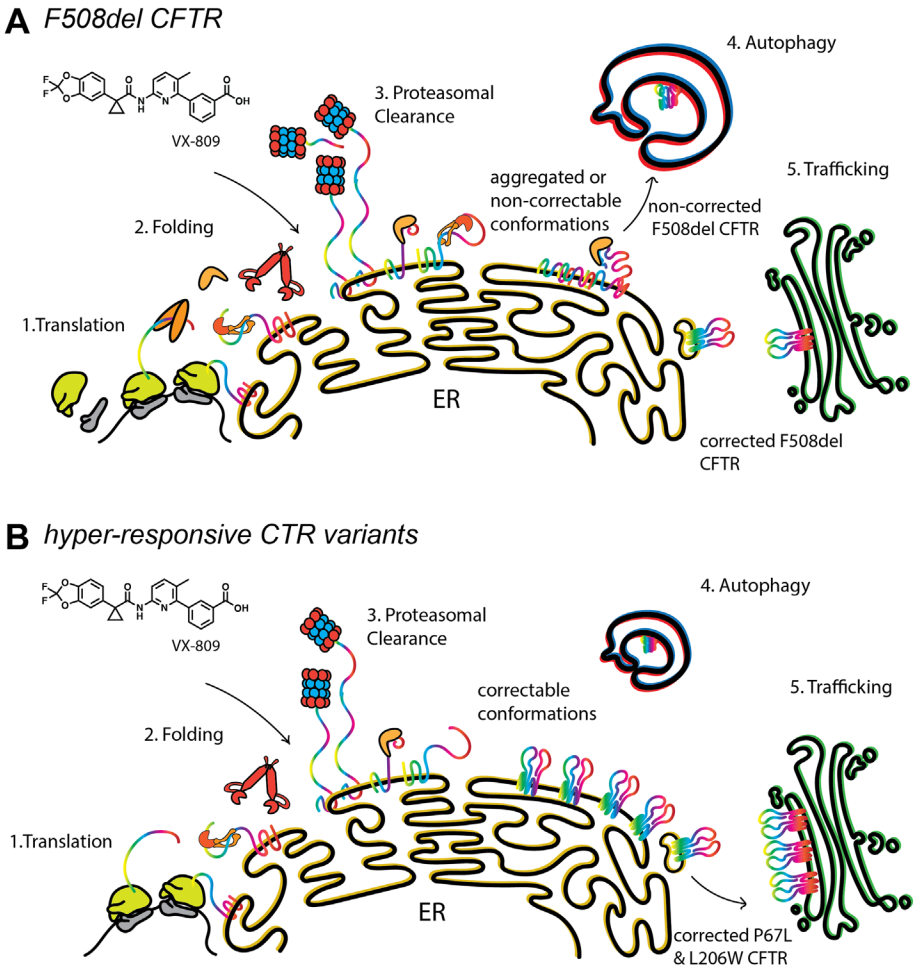

FIGURE 7: Model of VX-809 producing an inflection point just prior to protein degradation that requires clearance of noncorrectable CFTR conformations. (A) Schematic indicating the protein quality control process for *moderate-responsive* variant F508del. VX-809 reduces F508del interactions with translation and folding proteins, however, not interactions with proteasomal degradation and autophagy proteins, and thus is likely producing an inflection point between folding and proteasomal degradation. Since inhibiting autophagy attenuates F508del VX-809 response, it is likely that autophagy clearance of noncorrectable conformations is required for VX-809 to correct F508del. (B) Schematic showing fates of *hyperresponsive* variants P67L and L206W. VX-809 reduced P67L and L206W interactions with translation, folding, proteasomal degradation, autophagy, and trafficking proteins allowing robust VX-809 response indicative in the increased trafficking. Since inhibiting proteasomal degradation attenuates P67L and L206W VX-809 response, it is likely that proteasomal clearance of noncorrectable conformations is required for VX-809 to correct P67L and L206W.

followed up by determining the interactome changes of two other mutants: *hyperresponsive* L206W, which represents a novel interactome not previously published, and *nonresponder* G85E. We showed VX-809 reduced L206W interactions globally across many pathways when compared with WT CFTR, confirming VX-809 correction remodels a near-WT interactome. By contrast, VX-809 does not appear to alter the G85E interactome in any pathway. Most of the interactions presented in this study were up-regulated compared with WT with DMSO. The exceptions include WT and L206W with VX809 (Supplemental Figure S3, A and B and Figure 5C). This is in contrast to previous studies which showed up-regulation and down-regulation of interactors compared with WT (Pankow *et al.*, 2015; Hutt *et al.*, 2018).

What can *hyperresponsive* CFTR mutations reveal about the VX-809 mechanism? P67L and L206W experience reduced interaction with degradation machinery and pathways downstream of folding compared with F508del. VX-809 corrects both full-length F508del CFTR at the plasma membrane (Eckford *et al.*, 2014) and nascent F508del CFTR during biogenesis (Van Goor *et al.*, 2011). Our data suggest that L206W and P67L are likely corrected by VX-809 binding early in biogenesis, consistent with proposed binding sites at TMD1 (Ren *et al.*, 2013) and the TMD1/ nucleotide binding domain (NBD1) interface (Loo and Clarke, 2017). Importantly, since CFTR degradation and folding occur cotranslationally (Du *et al.*, 2005; Kleizen *et al.*, 2005) and likely before trafficking, we speculate reduction in trafficking proteins occurs after reduction of degradation machinery. Thus we propose a model where VX-809 produces an inflection point in biogenesis before routing toward proteasomal degradation (Figure 7A).

Recently, He *et al.* showed that N1303K CFTR is degraded by ER-associated autophagy involving DNAJB12 and they speculated that N1303K may not be retrotranslocatable (He *et al.*, 2021). By contrast, they showed that P67L/N1303K CFTR is not detected in autolysosomes and likely degraded proteasomally (He *et al.*, 2021). However, when treated with VX-809, P67L/N1303K is reverted back to ER-associated autophagy similar to N1303K (He *et al.*, 2021). This suggests that P67L is corrected by VX-809 at a step before autolysosomal degradation pathways (Figure 7B). However, precisely when this step occurs during CFTR folding remains unclear. We previously showed that the P67L VX-809 response requires the CFTR C terminus (Sabusap *et al.*, 2021). Chaperones such as DNAJB12 evaluate CFTR N-terminal/C-terminal interactions (Grove *et al.*, 2009). DNAJB12 has been shown to triage F508del CFTR through proteasomal degradation (Younger *et al.*, 2006; Grove *et al.*, 2011) and N1303K CFTR through autophagy (He *et al.*, 2021). Indeed, we see that P67L-DNAJB12 interactions are particularly reduced among folding factors by VX-809 when correlating the interaction fold changes (Supplemental Figure S4B). Furthermore, Hsp40 and Hsp70 chaperones bind the TMD2/lasso motif interface (Baaklini *et al.*, 2020) near P67L. Thus we speculate VX-809 rescues P67L during a chaperone-engaged conformation that is still susceptible to retrotranslocation and proteasomal degradation. This likely occurs when N-terminal/C-terminal interactions between the lasso motif/TMD2 are forming, which are perturbed in P67L but rescued by VX-809 (Sabusap *et al.*, 2021). We can only speculate on the precise folding events at which VX-809 becomes crucial for *hyperresponsive* mutations, but our data suggest VX-809 produces an inflection point during or just prior to proteasomal degradation.

We revealed in this study that VX-809 becomes crucial for *hyperresponsive* mutations before proteasomal degradation. Furthermore, we demonstrated that proteasome inhibition attenuates

P67L and L206W VX-809 response. These data suggest that proteasomal clearance is required to maintain a steady-state population of VX-809 correctable CFTR (Figure 7B). Mutant CFTR may be more prone to aggregation, thus requiring proteasomal clearance for a steady-state correctable population. This correctable CFTR population may be chaperone bound, undergoing posttranslational folding, and near a critical step in N-terminal/C-terminal interdomain assembly.

VX-809 *hyperresponsive* CFTR variants P67L and L206W share several commonalities. We measured the novel L206W interactome, revealing that L206W shares similar proteostasis interactions as other class-II mutations and the interactome of nonresponder G85E. We showed that VX-809 reduced L206W interactions globally across many pathways indicating VX-809 correction results in an almost near-WT interactome. By contrast, VX-809 does not appear to alter the G85E interactome in any pathway. On a pathway-specific basis, VX-809 reduced L206W with folding, translational, proteasomal, autophagy, and trafficking machinery. Thus L206W is likely corrected by VX-809 binding early in biogenesis, consistent with notions of TMD1 (Ren *et al.*, 2013) and the TMD1/NBD1 interface (Loo and Clarke, 2017) binding sites. By contrast, since G85 only interacts with residues in TMD1 (Supplemental Figure S5F), it is likely that a mutation here experiences misfolding early in biogenesis and cannot reach a correctable conformation by slowing membrane insertion (Patrick *et al.*, 2011). This is consistent with our Western blots showing that proteasomal inhibition increases G85E C band but does not synergize with VX-809. This suggests that some structural defects may simply be uncorrectable and possibly such defects precede protein interaction alterations. Alternatively, protein levels may contribute to rescue of hyperresponsive variants. P67L and L206W demonstrate higher residual function in patients (Figure 1A) and consequently may also present higher levels of protein available for rescue at steady state.

Thus VX-809 *hyperresponsive* CFTR mutants most likely reach a correctable conformation before the checkpoint to route for proteasomal degradation. Mechanistic studies of how the corrector changes CFTR interactions provide valuable information of a possible drug mechanism. Our TMT labeling approach provides a foundation for future work using a variety of CFTR mutations and corrector to theratype mutants.

Besides VX-809, additional pharmacologic corrector drugs are now in clinical use, including the combination treatment Trikafta, which was FDA approved in 2019. Trikafta contains the potentiator VX-770 (Ivacaftor) and two corrector compounds: VX-661 (Tezacaftor), which is a structural analog of VX-809, and VX-445 (Elexacaftor). The combination treatment is currently approved for patients carrying F508del hetero- and homozygous CFTR variants (nearly 90% of CF patients); however, many rare CFTR variants are not included in this list (Middleton *et al.*, 2019). Elucidation of the corrector theratypes for rare CFTR mutants and a better understanding of the principles that dictate their susceptibility to individual corrector compounds could broaden their therapeutic use for personalized CF medicine. Our multiplexed approach will facilitate the high-throughput characterization of altered proteostasis interactions of theratypes for future CFTR correctors. Beyond theratyping CFTR mutants, our high-throughput multiplexed TMT quantification approach offers the capability to theratype mutant protein variants associated with other protein misfolding diseases and respective pharmacologic chaperones.

MATERIALS AND METHODS

Request a protocol through *Bio-protocol*.

Plasmids and antibodies

Plasmids expressing CFTR in the pcDNA5 vector were gifted from E. Sorscher and J. Hong (Emory University, Atlanta, Georgia) (Sabusap *et al.*, 2016). Anti-CFTR mouse monoclonal antibodies included 217 R-domain antibodies (http://cftrantibodies.web.unc.edu/) (provided by J. Riordan, University of North Carolina, Chapel Hill, North Carolina) and 24-1 anti–C-terminus monoclonal antibodies (mAB 24-1 (ATCC HB-11947) purified from B lymphocyte hybridoma cells using a recombinant Protein G–Sepharose 4B Affinity Column on an ÄKTA start protein purification system (GE Life Science Product # 29022094). Antibodies were used in immunoblotting buffer (5% bovine serum albumin [BSA] in Tris-buffered saline, pH 7.5, 0.1% Tween-20, and 0.1% NaN_3) with 217 at 1:1000 dilutions. Secondary antibodies were obtained from commercial sources and used at the indicated dilutions in 5% milk in Tris-buffered saline (TBS), 0.1% Tween-20 (TBS-T): goat anti-mouse Starbright700 (1:10000, Bio-Rad), anti-rabbit rhodamine–conjugated tubulin (1:10000, Bio-Rad).

Immunoblotting, SDS–PAGE, and immunoprecipitation

HEK293T cells were transiently transfected with respective CFTR expression plasmids using a calcium phosphate method (Welzel *et al.*, 2004). A fully confluent 10-cm plate (approximately 10^7 cells) was used per condition. Cells were harvested by washing with phosphate-buffered saline (PBS) and incubated with 600 µl of TN buffer (50 mM Tris, pH 7.5, 150 mM NaCL) with 0.5% IGEPAL CA-630 and complete, Mini, EDTA-free protease inhibitor cocktail (Roche) in PBS and rocked at 4°C for 20 min. A cell scraper was then used to dislodge cells and transfer them to a microcentrifuge tube. Cells were sonicated for 3 min and spun down at 18,000 × *g* for 30 min. Total protein concentration was normalized using Bio-Rad protein assay dye. A 30 µl sample of the lysates (used as the "input") was then denatured with 20 µl 6× Laemmli buffer at room temperature for 1 hour, then incubated at 37°C for 15 min, followed by addition of 6 µl of 6× Laemmli buffer + 100 mM dithiothreitol and heated at 37°C for 15 min before being separated by SDS–PAGE. Samples were transferred onto PVDF membranes (Millipore) for immunoblotting and dehydrated. Primary antibodies were incubated either at room temperature for 2 h or overnight at 4°C. Membranes were then washed three times with TBS-T and incubated with secondary antibody constituted in 5% milk at 4°C for 1 h. Membranes were washed three times with TBS-T and then imaged using a ChemiDoc MP Imaging System (Bio-Rad).

CoPIT, developed by Pankow *et al.* was employed for AP of CFTR bound with interactors as described previously (Pankow *et al.*, 2016). Briefly, for immunoprecipitation, cell lysates were precleared with 4B Sepharose beads (Sigma) at 4°C for 1 h while rocking. Precleared lysates were then immunoprecipitated with Protein G beads complexed to the 24-1 antibody (6 mg antibody per ml of beads) overnight at 4°C while rocking. The next day, a sample of the supernatant was collected for Western blot analysis as the "clear" indicating residual protein not isolated by the beads. Resin was washed three times with TNI buffer, washed twice with TN buffer, and frozen at –80°C for 1.5 h. Proteins were then eluted twice with shaking at 37°C for 20 min–1 h with a 0.2 M glycine (pH 2.3)/0.5% IGEPAL CA-630 buffer. Samples were then blotted as described above or processed for MS analysis.

For Co-IP Western blots to identify and confirm interacting proteins the same procedure described above was used. Input and clear blots were probed with CFTR antibody to confirm successful immunoprecipitation. Elution blots were probed with PSMC3 polyclonal rabbit antibody (24142-1-AP) from Proteintech, EPR3c56

BAG2 rabbit antibody (ab79406) from Abcam, Derlin-1 rabbit antibody (ab176732) from Abcam, calnexin (c3) rabbit antibody from Genetex, and 217 CFTR mouse antibody in that order. All antibodies were diluted 1:1000 in 5% BSA in TBS with 0.1% Tween detergent.

Multiplexed LC-MS/MS

Eluted samples were precipitated in methanol/chloroform, washed three times with methanol, and air-dried. Protein pellets were then resuspended in 3 µl 1% Rapigest SF Surfactant (Waters) followed by the addition of 10 µl of 50 mM HEPES, pH 8.0, and 32.5 µl of H_2O. Samples were reduced with 5 mM tris(2-carboxyethyl)phosphine (Sigma) and alkylated with 10 mM iodoacetamide (Sigma); 0.5 µg of trypsin (Sequencing Grade, Promega, or Pierce) was then added and incubated for 16–18 h at 37°C with shaking at 700 rpm. Peptide samples were then reacted with TMT 11-plex reagents (Thermo Fisher) in 40% vol/vol acetonitrile and incubated for 1 h at room temperature. Reactions were then quenched by the addition of ammonium bicarbonate (0.4% wt/vol final concentration) and incubated for 1 h at room temperature. TMT-labeled samples for a given experiment were then pooled and acidified with 5% formic acid (Sigma, vol/vol). Samples were concentrated using a SpeedVac and resuspended in buffer A (95% water, 4.9% acetonitrile, and 0.1% formic acid, vol/vol/v). Cleaved Rapigest SF surfactant was removed by centrifugation for 30 min at 21,100 × *g*. Peptides were directly loaded onto a triphasic MudPIT columns using a high-pressure chamber. Samples were then washed for 30 min with buffer A. LC-MS/MS analysis was performed using an Exploris 480 (Thermo Fisher) mass spectrometer equipped with an UltiMate3000 RSLCnano System (Thermo Fisher). MudPIT experiments were performed with 10 µl sequential injections of 0, 10, 30, 60, and 100% buffer C (500 mM ammonium acetate in buffer A), followed by a final injection of 90% buffer C with 10% buffer B (99.9% acetonitrile, 0.1% formic acid vol/vol) and each step followed by a 90-min gradient from 4 to 40% B with a flow rate of either 300 or 500 nl/min, followed by a 15-min gradient from 40 to 80% B with a flow rate of 500 nl/min on a 20-cm fused silica microcapillary column (ID 100 µM) ending with a laser-pulled tip filled with Aqua C18, 3 µm, 100 Å resin (Phenomenex). Electrospray ionization was performed directly from the analytical column by applying a voltage of 2.0 or 2.2 kV with an inlet capillary temperature of 275°C. Data-dependent acquisition of MS/MS spectra was performed by scanning from 300 to 1800 m/z with a resolution of 60,000 to 120,000. Peptides with an intensity above 1.0E4 with charge state 2–6 from each full scan were fragmented by HCD using normalized collision energy of 35 to 38 with a 0.4 m/z isolation window, 120 ms maximum injection time at a resolution of 15,000–45,000, scanned from 100 to 1800 m/z or defined a first mass at 110 m/z and dynamic exclusion set to 45 or 60s and a mass tolerance of 10 ppm.

Interactome characterization

Peptide identification and TMT-based protein quantification was carried out using Proteome Discoverer 2.4. MS/MS spectra were extracted from Thermo XCaliber .raw file format and searched using SEQUEST against a UniProt human proteome database (released 03/25/2014) containing 20,337 protein entries. The database was curated to remove redundant protein and splice-isoforms and supplemented with common biological MS contaminants. Searches were carried out using a decoy database of reversed peptide sequences and the following parameters: 10 ppm peptide precursor tolerance, 0.02 Da fragment mass tolerance, minimum peptide length of six amino acids, trypsin cleavage with a maximum of two missed cleavages, static cysteine modification of 57.0215 (carbamidomethylation), and static N-terminal and lysine modifications of 229.1629 (TMT sixplex). SEQUEST search results were filtered using Percolator to minimize the peptide false discovery rate to 1% and a minimum of two peptides per protein identification. TMT reporter ion intensities were quantified using the Reporter Ion Quantification processing node in Proteome Discoverer 2.4 and summed for peptides belonging to the same protein.

Proteostasis modulator experiments

Western blot analysis was performed on P67L, L206W, G85E, and F508del CFTR under a combination of VX-809 and proteostasis modulator conditions. A 10-cm dish was transiently transfected with 4 µg of the respective CFTR mutation using calcium phosphate transfection described previously. After 16 h the media was changed and left to incubate for 1 h. Next, the 10-cm dish was split using 1 ml trypsin and 5 ml media to inoculate a 6-well dish with 1 ml of transfected cells such that the transfection efficiency was the same across the conditions. Next, 2 µl of 3 mM VX-809 was added to respective wells of the 6-well dish for a final concentration of 3 µM. Then, each column of the 6-well dish was treated with DMSO, 10 µM bortezomib, or 10 µM E-64, respectively. Cells were collected 12–16 h after treatment, lysed, normalized, and run for Western blotting as described above.

Pathway analysis/selection of biological pathway from GOterms on Uniprot

First, we searched our dataset against the pathway classification presented by Pankow *et al*. (2015). This step classified all previously identified interactors. For novel interactors we manually annotated pathways by searching gene names on UniProt and classifying pathways by GO-terms for Biological Pathway.

Statistical analysis

To determine statistically significant CFTR interaction proteins, we used a two-tailed paired *t* test (using the scipy.stats.ttest_rel package in Python) to calculate the *p* value between the log2 TMT intensity of each protein pulled down with CFTR and the corresponding the log2 TMT intensity of each protein pulled down with tdTomato control. First, we normalized log2 protein abundances to the log2 CFTR protein abundance across TMT channels in individual TMT-11plex sets (Supplemental Figure S2). We then scaled the log2-fold abundances for these interactors to the corresponding WT DMSO condition within each run to provide a common reference point. Subsequently, we averaged these scaled log2 abundance changes from replicate TMT11plex sets. Finally, we excluded any proteins not quantified for both WT and F508del since direct quantitative comparison is not possible for these proteins. A heatmap portraying all proteins included for all pathways and all mutants showing this normalization is included (Supplemental Figure S3B) as well as the data plotted (Supplement Dataset 3). For aggregate pathways statistics in violin plots, we used a one-way ANOVA with Geisser-Greenhouse correction and post-hoc Tukey multicomparison testing to evaluate the statistically significant difference between conditions for a given pathway. Data plotted are included (Supplement Dataset 4). Finally, we used a two-tailed ratio paired *t* test to determine statistical differences between quantified Western blot data.

ACKNOWLEDGMENTS

We thank Eric Sorscher and Jeong Wong (Emory University, Atlanta, Georgia, USA) for CFTR expression plasmids. We thank members of the Plate lab for their critical reading and feedback on this manuscript. This work was funded by T32 GM065086 (NIGMS) (EFM); the

Cystic Fibrosis Foundation Postdoctoral Fellowship (SABUSA19F0) (CMPS); R35 GM133552 (NIGMS); and Vanderbilt University funds.

REFERENCES

Alberti S, Böhse K, Varndt E, Schmitz A, Höhfeld J (2004). The cochaperone HspBP1 inhibits the CHIP ubiquitin ligase and stimulates the maturation of the cystic fibrosis transmembrane conductance regulator. Mol Biol Cell 15, 5565–5573.

Anglès F, Hutt DM, Balch WE (2018). HDAC inhibitors rescue multiple disease-causing CFTR variants. Hum Mol Genet 28, 1982–2000.

Arndt V, Daniel C, Nastainczyk W, Alberti S, Höhfeld J (2005). BAG-2 acts as an inhibitor of the chaperone-associated ubiquitin ligase CHIP. Mol Biol Cell 16, 5891–5900.

Baaklini I, de Gonçalves CC, Lukacs GL, Young JC (2020). Selective binding of HSC70 and its co-chaperones to structural hotspots on CFTR. Sci Rep 10, 4176.

Baatallah N, Elbahnsi A, Mornon JP, Chevalier B, Pranke I, Servel N, Zelli R, Décout JL, Edelman A, Sermet-Gaudelus I, *et al.* (2021). Pharmacological chaperones improve intra-domain stability and inter-domain assembly via distinct binding sites to rescue misfolded CFTR. Cell Mol Life Sci, 78, 7813–7829.

Barrett AJ, Kembhavi AA, Brown MA, Kirschke H, Knight CG, Tamai M, Hanada K (1982). L-trans-Epoxysuccinyl-leucylamido(4-guanidino)butane (E-64) and its analogues as inhibitors of cysteine proteinases including cathepsins B, H and L. Biochem J 201, 189–198.

(CFTR2.org) , TC and FTr of C CFTR2.

Clain J, Lehmann-Che J, Duguépéroux I, Arous N, Girodon E, Legendre M, Goossens M, Edelman A, de Braekeleer M, Teulon J, *et al.* (2005). Misprocessing of the CFTR protein leads to mild cystic fibrosis phenotype. Hum Mutat 25, 360–371.

Clancy JP, Cotton CU, Donaldson SH, Solomon GM, VanDevanter DR, Boyle MP, Gentzschg M, Nick JA, Illek B, Wallenburg JC, *et al.* (2019). CFTR modulator theratyping: Current status, gaps and future directions. J Cyst Fibros 18, 22–34.

Coppinger JA, Hutt DM, Razvi A, Koulov AV, Pankow S, Yates JR, Balch WE (2012). A chaperone trap contributes to the onset of cystic fibrosis. PLoS One 7, 17–19.

Craig EA (2018). Hsp70 at the membrane: Driving protein translocation. BMC Biol 16.

Davies JP, Almasy KM, McDonald EF, Plate L (2020). Comparative multiplexed interactomics of SARS-CoV-2 and homologous coronavirus nonstructural proteins identifies unique and shared host-cell dependencies. ACS Infect Dis 6, 3174–3189.

Du K, Sharma M, Lukacs GL (2005). The ΔF508 cystic fibrosis mutation impairs domain-domain interactions and arrests post-translational folding of CFTR. Nat Struct Mol Biol 12, 17–25.

Eckford PDW, Ramjeesingh M, Molinski S, Pasyk S, Dekkers JF, Li C, Ahmadi S, Ip W, Chung TE, Du K, *et al.* (2014). VX-809 and related corrector compounds exhibit secondary activity stabilizing active F508del-CFTR after its partial rescue to the cell surface. Chem Biol 21, 666–678.

Farinha CM, King-Underwood J, Sousa M, Correia AR, Henriques BJ, Roxo-Rosa M, Da Paula AC, Williams J, Hirst S, Gomes CM, *et al.* (2013). Revertants, low temperature, and correctors reveal the mechanism of F508del-CFTR rescue by VX-809 and suggest multiple agents for full correction. Chem Biol 20, 943–955.

Farinha CM, Amaral MD (2005). Most F508del-CFTR is targeted to degradation at an early folding checkpoint and independently of calnexin. Mol Cell Biol 25, 5242–5252.

Farinha CM, Canato S (2017). From the endoplasmic reticulum to the plasma membrane: mechanisms of CFTR folding and trafficking. Cell Mol Life Sci 74, 39–55.

Fiedorczuk K, Chen J (2022). Mechanism of CFTR correction by type I folding correctors. Cell 185, 158–168.e11.

Grove DE, Fan C-Y, Ren HY, Cyr DM (2011). The endoplasmic reticulum–associated Hsp40 DNAJB12 and Hsc70 cooperate to facilitate RMA1 E3–dependent degradation of nascent CFTRΔF508. Mol Biol Cell 22, 301–314.

Grove DE, Rosser MFN, Ren HY, Naren AP, Cyr DM (2009). Mechanisms for rescue of correctable folding defects in CFTRΔF508. Mol Biol Cell 20, 4059–4069.

Han ST, Rab A, Pellicore MJ, Davis EF, McCague AF, Evans TA, Joynt AT, Lu Z, Cai Z, Raraigh KS, *et al.* (2018). Residual function of cystic fibrosis mutants predicts response to small molecule CFTR modulators. JCI Insight 3, e121159.

He L, Kennedy AS, Houck S, Aleksandrov A, Quinney NL, Cyr-Scully A, Cholon DM, Gentzsch M, Randell SH, Ren HY, *et al.* (2021). DNAJB12 and Hsp70 triage arrested intermediates of N1303K-CFTR for endoplasmic reticulum-associated autophagy. Mol Biol Cell 32, 538–553.

Hegde RN, Parashuraman S, Iorio F, Ciciriello F, Capuani F, Carissimo A, Carrella D, Belcastro V, Subramanian A, Bounti L, *et al.* (2015). Unravelling druggable signalling networks that control F508del-CFTR proteostasis. Elife 4, 1–28.

Hegedus T, Aleksandrov A, Cui L, Gentzsch M, Chang XB, Riordan JR (2006). F508del CFTR with two altered RXR motifs escapes from ER quality control but its channel activity is thermally sensitive. Biochim Biophys Acta - Biomembr 1758, 565–572.

Heijerman HGM, McKone EF, Downey DG, Van Braeckel E, Rowe SM, Tullis E, Mall MA, Welter JJ, Ramsey BW, McKee CM, *et al.* (2019). Efficacy and safety of the elexacaftor plus tezacaftor plus ivacaftor combination regimen in people with cystic fibrosis homozygous for the F508del mutation: a double-blind, randomised, phase 3 trial. Lancet (London, England) 6736, 6–14.

Horváth I, Multhoff G, Sonnleitner A, Vígh L (2008). Membrane-associated stress proteins: More than simply chaperones. Biochim Biophys Acta - Biomembr 1778, 1653–1664.

Hutt DM, Loguercio S, Campos AR, Balch WE (2018). A proteomic variant approach (ProVarA) for personalized medicine of inherited and somatic disease. J Mol Biol 430, 2951–2973.

Kim SJ, Skach WR (2012). Mechanisms of CFTR folding at the endoplasmic reticulum. Front Pharmacol 3, 201.

Kleizen B, Van Vlijmen T, De Jonge HR, Braakman I (2005). Folding of CFTR is predominantly cotranslational. Mol Cell 20, 277–287.

Lim SH, Legere EA, Snider J, Stagljar I (2018). Recent progress in CFTR interactome mapping and its importance for cystic fibrosis. Front Pharmacol 8, 1–9.

Lin JH, Li H, Yasumura D, Cohen HR, Zhang C, Panning B, Shokat KM, Lavail MM, Walter P (2007). IRE1 signaling affects cell fate during the unfolded protein response. Science 318, 944–949.

Loo MA, Jensen TJ, Cui L, Hou YX, Chang XB, Riordan JR (1998). Perturbation of Hsp90 interaction with nascent CFTR prevents its maturation and accelerates its degradation by the proteasome. EMBO J 17, 6879–6887.

Loo TW, Clarke DM (2017). Corrector VX-809 promotes interactions between cytoplasmic loop one and the first nucleotide-binding domain of CFTR. Biochem Pharmacol 136, 24–31.

Lopes-Pacheco M, Boinot C, Sabirzhanova I, Rapino D, Cebotaru L (2017). Combination of correctors rescues CFTR transmembrane-domain mutants by mitigating their interactions with proteostasis. Cell Physiol Biochem 41, 2194–2210.

Manfredi C, Tindall JM, Hong JS, Sorscher EJ (2019). Making precision medicine personal for cystic fibrosis. Science (80-) 365, 220–221.

McAlister GC, Huttlin EL, Haas W, Ting L, Jedrychowski MP, Rogers JC, Kuhn K, Pike I, Grothe RA, Blethrow JD, *et al.* (2012). Increasing the multiplexing capacity of TMTs using reporter ion isotopologues with isobaric masses. Anal Chem 84, 7469–7478.

Middleton PG, Mall MA, Dřevínek P, Lands LC, McKone EF, Polineni D, Ramsey BW, Taylor-Cousar JL, Tullis E, Vermeulen F, *et al.* (2019). Elexacaftor–Tezacaftor–Ivacaftor for cystic fibrosis with a single Phe508del allele. N Engl J Med 381, 1809–1819.

Molinski SV, Shahani VM, Subramanian AS, MacKinnon SS, Woollard G, Laforet M, Laselva O, Morayniss LD, Bear CE, Windemuth A (2018). Comprehensive mapping of cystic fibrosis mutations to CFTR protein identifies mutation clusters and molecular docking predicts corrector binding site. Proteins Struct Funct Bioinforma 86, 833–843.

Molinski SV, Ahmadi S, Ip W, Ouyang H, Villella A, Miller JP, Lee PS, Kulleperuma K, Du K, Di Paola M, *et al.* (2017). Orkambi® and amplifier co-therapy improves function from a rareCFTRmutation in gene-edited cells and patient tissue. EMBO Mol Med 9, 1224–1243.

Obeng EA, Carlson LM, Gutman DM, Harrington Jr, WJ, Lee KP, Boise LH (2006). Proteasome inhibitors induce a terminal unfolded protein response in multiple myeloma cells. Blood 107, 4907–4916.

Okiyoneda T, Barrière H, Bagdány M, Rabeh WM, Du K, Höhfeld J, Young JC, Lukacs GL (2010). Peripheral protein quality control removes unfolded CFTR from the plasma membrane. Science (80-) 329, 805–810.

Okiyoneda T, Veit G, Dekkers JF, Bagdany M, Soya N, Xu H, Roldan A, Verkman AS, Kurth M, Simon A, *et al.* (2013). Mechanism-based corrector combination restores ΔF508-CFTR folding and function. Nat Chem Biol 9, 444–454.

Oliver KE, Rauscher R, Mijnders M, Wang W, Wolpert MJ, Maya J, Sabusap CM, Kesterson RA, Kirk KL, Rab A, *et al.* (2019). Slowing ribosome

velocity restores folding and function of mutant CFTR. J Clin Invest 129, 5236–5253.
Pankow S, Bamberger C, Calzolari D, Bamberger A, Yates III, JR (2016). Deep interactome profiling of membrane proteins by co-interacting protein identification technology. Nat Protoc 11, 2515.
Pankow S, Bamberger C, Calzolari D, Martínez-Bartolomé S, Lavallée-Adam M, Balch WE, Yates JR III (2015). ΔF508 CFTR interactome remodeling promotes rescue of cystic fibrosis. Nature 528, 510.
Paramore A, Frantz S (2003). Bortezomib. Nat Rev Drug Discov 2, 611+.
Patrick AE, Karamyshev AL, Millen L, Thomas PJ (2011). Alteration of CFTR transmembrane span integration by disease-causing mutations. Mol Biol Cell 22, 4461–4471.
Plate L, Rius B, Nguyen B, Genereux JC, Kelly JW, Wiseman RL (2019). Quantitative interactome proteomics reveals a molecular basis for ATF6-dependent regulation of a destabilized amyloidogenic protein. Cell Chem Biol 26, 913–925.e4.
Ren HY, Grove DE, De LaRosa O, Houck SA, Sopha P, Van Goor F, Hoffman BJ, Cyr DM (2013). VX-809 corrects folding defects in cystic fibrosis transmembrane conductance regulator protein through action on membrane-spanning domain 1. Mol Biol Cell 24, 3016–3024.
Rosser MFN, Grove DE, Chen L, Cyr DM (2008). Assembly and misassembly of cystic fibrosis transmembrane conductance regulator: folding defects caused by deletion of F508 occur before and after the calnexin-dependent association of membrane spanning domain (MSD) 1 and MSD2. Mol Biol Cell 20, 2673–2683.
Rowe SM, Miller S, Sorscher EJ (2005). Cystic fibrosis. N Engl J Med 352, 1992–2001.
Rozen R, Ferreira-Rajabi L, Robb L, Colman N (1995). L206W mutation of the cystic fibrosis gene, relatively frequent in French Canadians, is associated with atypical presentations of cystic fibrosis. Am J Med Genet 57, 437–439.
Sabusap CM, Joshi D, Simhaev L, Oliver KE, Senderowitz H, van Willigen M, Braakman, I, Rab A, Sorscher EJ, Hong JS (2021). The CFTR P67L variant reveals a key role for N-terminal lasso helices in channel folding, maturation, and pharmacologic rescue. J Biol Chem, 100598.
Sabusap CM, Wang W, McNicholas CM, Chung WJ, Fu L, Wen H, Mazur M, Kirk KL, Collawn JF, Hong JS, *et al*. (2016). Analysis of cystic fibrosis–associated P67L CFTR illustrates barriers to personalized therapeutics for orphan diseases. JCI Insight 1, 1–10.
Santos JD, Canato S, Carvalho AS, Botelho HM, Aloria K, Amaral MD, Matthiesen R, Falcao AO, Farinha CM (2019). folding status is determinant over traffic-competence in defining CFTR interactors in the endoplasmic reticulum. Cells 8, 353.
Sun F, Zhang R, Gong X, Geng X, Drain PF, Frizzell RA (2006). Derlin-1 promotes the efficient degradation of the cystic fibrosis transmembrane conductance regulator (CFTR) and CFTR folding mutants. J Biol Chem 281, 36856–36863.
Van Goor F, Hadida S, Grootenhuis PDJ, Burton B, Stack JH, Straley KS, Decker CJ, Miller M, McCartney J, Olson ER, *et al*. (2011). Correction of the F508del-CFTR protein processing defect in vitro by the investigational drug VX-809. Proc Natl Acad Sci 108, 18843–18848.
Van Goor F, Straley KS, Cao D, González J, Hadida S, Hazlewood A, Joubran J, Knapp T, Makings LR, Miller M, *et al*. (2006). Rescue of ΔF508-CFTR trafficking and gating in human cystic fibrosis airway primary cultures by small molecules. Am J Physiol Cell Mol Physiol 290, L1117–L1130.
Veit G, Avramescu RG, Chiang AN, Houck SA, Cai Z, Peters KW, Hong JS, Pollard HB, Guggino WB, Balch WE, *et al*. (2016). From CFTR biology toward combinatorial pharmacotherapy: expanded classification of cystic fibrosis mutations. Mol Biol Cell 27, 424–433.
Veit G, Xu H, Dreano E, Avramescu RG, Bagdany M, Beitel LK, Roldan A, Hancock MA, Lay C, Li W, *et al*. (2018). Structure-guided combination therapy to potently improve the function of mutant CFTRs. Nat Med 24, 1732–1742.
Vertex pharmaceuticals incorporated Who is TRIKAFTA® For? | TRIKAFTA® (elexacaftor/tezacaftor/ivacaftor and ivacaftor). https://www.trikafta.com/who-trikafta-is-for
Vertex Pharmaceuticals Incorporated (2020a). ORKAMBI® (lumacaftor/ivacaftor) | Patient Information. https://www.orkambi.com/
Vertex Pharmaceuticals Incorporated (2020b). Who is KALYDECO® For? | KALYDECO® (ivacaftor). https://www.kalydeco.com/who-kalydeco
Vertex Pharmaceuticals Incorporated (2020c). Who SYMDEKO® (tezacaftor/ivacaftor and ivacaftor) Is For. https://www.symdeko.com/who-symdeko-is-for
Wainwright CE, Elborn JS, Ramsey BW, Marigowda G, Huang X, Cipolli M, Colombo C, Davies JC, De Boeck K, Flume PA, *et al*. (2015). Lumacaftor–Ivacaftor in patients with cystic fibrosis homozygous for Phe508del *CFTR*. N Engl J Med 373, 220–231.
Wang X, Venable J, LaPoint P, Hutt DM, Koulov AV, Coppinger J, Gurkan C, Kellner W, Matteson J, Plutner H, *et al*. (2006). Hsp90 Cochaperone Aha1 downregulation rescues misfolding of CFTR in cystic fibrosis. Cell 127, 803–815.
Welzel T, Radtke I, Meyer-Zaika W, Heumann R, Epple M (2004). Transfection of cells with custom-made calcium phosphate nanoparticles coated with DNA. J Mater Chem 14, 2213–2217.
Westhoff B, Chapple JP, Van Der Spuy J, Höhfeld J, Cheetham ME (2005). HSJ1 is a neuronal shuttling factor for the sorting of chaperone clients to the proteasome. Curr Biol 15, 1058–1064.
Wright MT, Kouba L, Plate L (2021). Thyroglobulin interactome profiling defines altered proteostasis topology associated with thyroid dyshormonogenesis. Mol Cell Proteomics 20, 100008.
Xi Y, Ju R, Wang Y (2020). Roles of Annexin A protein family in autophagy regulation and therapy. Biomed Pharmacother 130, 110591.
Younger JM, Chen L, Ren HY, Rosser MFN, Turnbull EL, Fan CY, Patterson C, Cyr DM (2006). Sequential Quality-Control Checkpoints Triage Misfolded Cystic Fibrosis Transmembrane Conductance Regulator. Cell 126, 571–582.